ERDC/GSL TR-12-26

Geotechnical and Structures Laboratory

US Army Corps
of Engineers®
Engineer Research and
Development Center

Laboratory Characterization of Adobe (Scottsdale)

Hannah B. Beatty, Steven S. Graham, Rayment E. Moxley,
Stephen A. Akers, and Paul A. Reed

July 2012

ERDC/GSL TR-12-26
July 2012

Laboratory Characterization of Adobe (Scottsdale)

Hannah B. Beatty, Steven S. Graham, Rayment E. Moxley,
Stephen A. Akers, and Paul A. Reed

Geotechnical and Structures Laboratory
U.S. Army Engineer Research and Development Center
3909 Halls Ferry Road
Vicksburg, MS 39180-6199

Final report

Prepared for Headquarters, U.S. Army Corps of Engineers
441 G Street, NW
Washington, DC 20314-1000

Under Hardened Combined Penetrator Warhead Technology Work Package
Scalable Technologies for Adaptive Response

Abstract

Personnel of the Geotechnical and Structures Laboratory, U.S. Army Engineer Research and Development Center, Vicksburg, Mississippi, conducted a laboratory investigation to characterize the strength and constitutive property behavior of an adobe from Scottsdale, Arizona. Twenty-one mechanical property tests, consisting of 12 triaxial compression (TXC) tests, two uniaxial strain (UX) tests, and seven unconfined compression (UC) tests, were successfully completed. In addition to the mechanical property tests, nondestructive pulse-velocity measurements were performed on each specimen. The TXC tests exhibited a continuous increase in maximum principal stress difference with increasing confining stress. A compression failure surface was developed from the UC and TXC test results. The UX stress-strain responses exhibited continuous increases in compaction up to the applied peak stresses and did not achieve full saturation.

Contents

Figures and Tables

Figures

Tables

Preface

This laboratory mechanical property investigation of Scottsdale adobe was conducted by personnel of the U.S. Army Engineer Research and Development Center (ERDC). Funding was provided by Headquarters, U.S. Army Corps of Engineers, under the Dynamic Behavior of Advanced Urban Materials Work Unit of the Scalable Technologies for Adaptive Response Work Package. This study was conducted in May 2010 by staff members of the Impact and Explosion Effects Branch (IEEB), Engineering Systems and Materials Division (ESMD), Geotechnical and Structures Laboratory (GSL), ERDC.

The Principal Investigator for this project was Dr. Stephen A. Akers. Hannah B. Beatty served as co-investigator for this project and processed the material property data with assistance from Steven S. Graham. Laboratory characterization tests were performed by Paul A. Reed under the technical direction of Akers. Beatty prepared this report.

During this research effort, Henry S. McDevitt Jr., was Chief, IEEB; Dr. Larry N. Lynch was Chief, ESMD; Dr. William P. Grogan was Deputy Director, GSL; and Dr. David W. Pittman was Director, GSL.

At the time of publication, COL Kevin J. Wilson was Commander and Executive Director of ERDC. Dr. Jeffery P. Holland was Director.

1 Introduction

Background

Personnel of the Geotechnical and Structures Laboratory, U.S. Army Engineer Research and Development Center (ERDC), conducted a laboratory investigation to characterize the strength and constitutive property behavior of Scottsdale adobe. ERDC personnel conducted 21 mechanical property tests, consisting of 12 triaxial compression tests, two uniaxial strain tests, and seven unconfined compression tests. The seven unconfined compression tests were performed only to establish the average unconfined compressive strength of the materials; therefore, no tabular data from these tests are included in this report. In addition to the mechanical property tests, nondestructive pulse-velocity measurements were performed on each specimen.

Purpose and scope

The purpose of this report is to document the results from the laboratory mechanical property tests and nondestructive pulse-velocity measurements conducted on the adobe specimens. The physical and composition properties, test procedures, and test results are documented in Chapter 2. Comparative plots and analyses of the experimental results are presented in Chapter 3. A summary is provided in Chapter 4.

2 Laboratory Tests

Material description

The test specimens used in this investigation were prepared by Old Pueblo Adobe Company, Inc., Scottsdale, Arizona. The samples were prepared by pouring the mix into 12.7-cm-long by 5.1-cm-diameter pipes. After the curing process was completed, the samples were shipped to ERDC. Additional details are documented in the Specimen Preparation section of this chapter.

Composition property tests

Prior to performing the mechanical property tests, the height, diameter, and weight for each test specimen were determined. These measurements were used to compute the specimen's wet, bulk, or as-tested density. Results from these determinations are provided in Table 1. Measurements of post-test water content[1] were conducted in accordance with procedures given in American Society for Testing and Materials (ASTM) D 2216 (ASTM 2009b). Based on the appropriate values of post-test water content, wet density, and an assumed grain density of 2.69 Mg/m^3, values of dry density, porosity, degree of saturation, and volumes of air, water, and solids were calculated (Table 1). Also listed in the table are maximum, minimum, and mean values and the standard deviation about the mean for each quantity. The adobe specimens had a mean wet density of 1.789 Mg/m^3, a mean water content of 1.05 percent, and a mean dry density of 1.77 Mg/m^3.

Ultrasonic pulse-velocity determinations

Prior to the performance of a mechanical property test, ultrasonic pulse-velocity measurements were collected on each test specimen. This involved measuring the transit distance and time for each P-wave (compressional) or S-wave (shear) pulse to propagate through a given specimen. The velocity then was computed by dividing the transit distance by the transit time.

[1] Water content is defined as the weight of water removed during drying in a standard oven divided by the weight of dry solids, then multiplied by 100.

Table 1. Physical and compositional properties of adobe.

Test Number	Type of Test	Plate Number	Wet Density, Mg/m^3	Posttest Water Content, %	Dry Density, Mg/m^3	Porosity, %	Degree of Saturation, %	Volume of Air, %	Volume of Water, %	Volume of Solids, %	Axial P Wave Velocity km/s	Radial P Wave Velocity km/s	Axial S Wave Velocity km/s	Radial S Wave Velocity km/s
1	TXC/5	1	1.815	1.070	1.796	33.29	5.77	31.37	1.92	66.71	1.674	2.060	1.013	1.252
2	TXC/5	2	1.789	0.920	1.772	34.15	4.77	32.52	1.63	65.85	1.736	2.191	1.037	1.206
3	TXC/10	3	1.713	1.120	1.694	37.08	5.12	35.18	1.90	62.92	2.113	1.998	1.003	1.251
4	TXC/10	4	1.827	0.960	1.810	32.77	5.30	31.03	1.74	67.23	1.666	2.118	0.990	1.200
5	TXC/20	5	1.729	0.960	1.713	36.36	4.52	34.72	1.64	63.64	1.654	1.944	0.970	1.145
6	TXC/20	6	1.799	0.950	1.782	33.81	5.01	32.11	1.69	66.19	1.848	2.145	1.079	1.264
7	TXC/50	7	1.714	1.200	1.694	37.06	5.49	35.03	2.03	62.94	1.787	2.121	1.084	1.293
8	TXC/50	8	1.842	1.060	1.823	32.28	5.98	30.35	1.93	67.72	1.722	2.112	1.015	1.230
9	TXC/100	9	1.825	1.040	1.806	32.90	5.71	31.02	1.88	67.10	2.186	2.033	1.007	1.207
10	TXC/100	10	1.777	1.160	1.757	34.73	5.87	32.69	2.04	65.27	1.684	2.170	1.050	1.281
11	TXC/200	11	1.802	1.140	1.781	33.82	6.00	31.79	2.03	66.18	2.148	1.997	1.016	1.187
12	TXC/200	12	1.819	1.080	1.800	33.14	5.86	31.20	1.94	66.86	1.684	2.133	1.014	1.197
13	UX	13	1.802	1.150	1.781	33.81	6.06	31.77	2.05	66.19	1.664	2.130	1.005	1.189
14	UX	14	1.793	0.930	1.776	34.01	4.86	32.36	1.65	65.99	2.038	2.046	1.039	1.194
N			14	14	14	14	14	14	14	14	14	14	14	14
Mean			1.789	1.053	1.770	34.23	5.45	32.37	1.86	65.77	1.829	2.086	1.023	1.221
Stdv			0.042	0.095	0.042	1.55	0.52	1.56	0.16	1.55	0.201	0.073	0.032	0.042
Max			1.842	1.200	1.823	37.08	6.06	35.18	2.05	67.72	2.186	2.191	1.084	1.293
Min			1.713	0.920	1.694	32.28	4.52	30.35	1.63	62.92	1.654	1.944	0.970	1.145

A matching pair of 1-MHz piezoelectric transducers was used to transmit and receive the ultrasonic P-waves. A pair of 2.25-MHz piezoelectric transducers was used to transmit and receive the ultrasonic S-waves. The transit time was measured with a 100-MHz digital oscilloscope and the transit distance with a digital micrometer. All of these wave-velocity determinations were made under atmospheric conditions (i.e., no pre-stress of any kind was applied to the specimens). The tests were conducted in accordance with procedures given in ASTM C 597 (ASTM 2009a).

One compressional-wave (P-wave) and one shear-wave (S-wave) velocity were determined axially through each specimen. Six radial P-wave velocities were determined (i.e., two transverse to each other at elevations of ¼, ½, and ¾ of the specimen height). Two radial S-wave velocities were measured; both of these measurements were made at the mid-height of the specimen transverse to each other. The various P- and S-wave velocities determined for the test specimens are provided in Table 1; the radial-wave velocities listed in Table 1 are the average values.

Mechanical property tests

Fourteen mechanical property tests on cylindrical specimens were performed successfully on the adobe specimens to characterize the strength and constitutive properties of the material. All of these tests were conducted quasi-statically with axial strain rates on the order of 10^{-4} to 10^{-5} per sec and times to peak load on the order of 5 to 30 min. Mechanical property data were obtained under several different stress and strain paths. Undrained compressibility data were obtained during the hydrostatic loading (HC) phase of the triaxial compression (TXC) tests. Shear and failure data were obtained from unconsolidated-undrained TXC tests. One-dimensional compressibility data were obtained from undrained uniaxial strain (UX), or K_0 tests, with lateral stress measurements or. The terms undrained and unconsolidated signify that no pore fluid (liquid or gas) was allowed to escape or drain from the membrane-enclosed specimens. The completed test matrix is presented in Table 2, which lists the types of tests conducted, the number of tests, the test numbers for each group, and the nominal peak radial stress applied to specimens prior to shear loading or during the HC or UX loading.

Table 2. Completed adobe test matrix.

Type of test	No. of tests	Test number	Nominal peak radial stress, MPa
	2	1, 2	5
	2	3, 4	10
	2	5, 6	20
	2	7, 8	50
	2	9, 10	100
Triaxial compression	2	11, 12	200
UX strain	2	13, 14	MAX (400)
Total # tests:	14		

Specimen preparation

The test specimens received from Old Pueblo were 12.7 cm long by 5.1 cm in diameter. They were cut to the correct length for mechanical property testing, and the ends were ground flat and parallel to each other and perpendicular to the sides of the core in accordance with procedures in ASTM D 4543 (ASTM 2009c). Prior to testing, the prepared specimens were measured for height, diameter, and weight and were ultrasonically pulsed. This information was used to calculate the composition properties and wave velocities of the specimens. The prepared test specimens had a nominal height of 110 mm and a nominal diameter of 50 mm.

Prior to testing, each specimen was placed between hardened steel top and base caps. Three or four 0.6-mm-thick latex membranes were placed around the test specimens (Figure 1). The exterior of the outside membrane was coated with a liquid synthetic rubber to inhibit deterioration caused by the confining-pressure fluid. The fluid was a mixture of kerosene and hydraulic oil. Finally, the specimen, along with its top and base caps, was placed on the instrumentation stand of the test apparatus, and the instrumentation setup was initiated.

Test devices

The tests were conducted in a 600-MPa-capacity pressure vessel (Figure 2), and an 8.9-MN loader provided the axial load. The applications of load, pressure, and axial displacement were regulated by a servo-controlled data acquisition system that allowed the user to program rates of load, pressure, and axial displacement to achieve the desired stress or strain path.

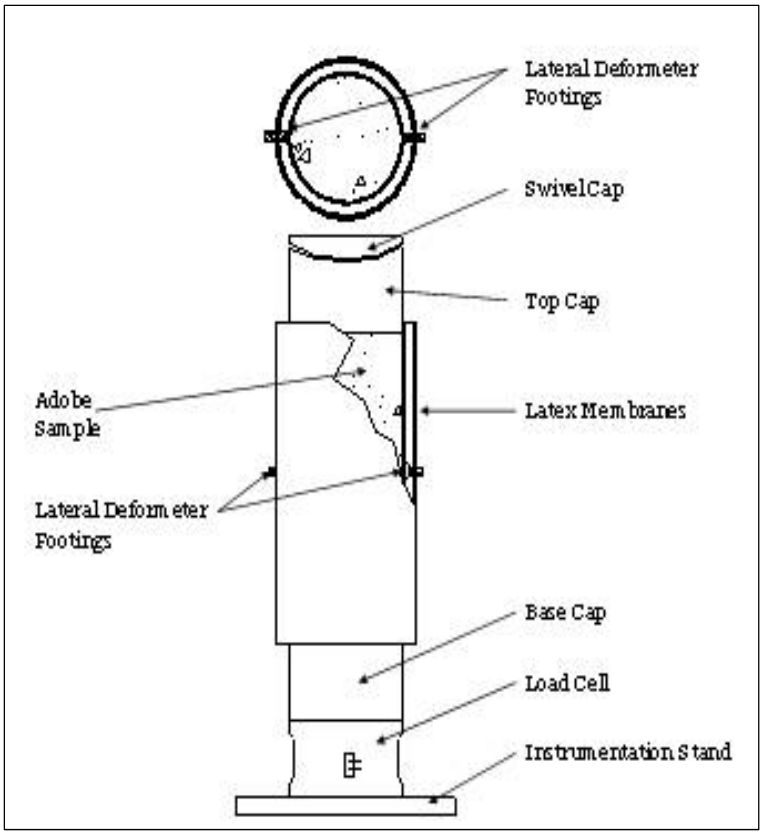

Figure 1. Typical test specimen setup.

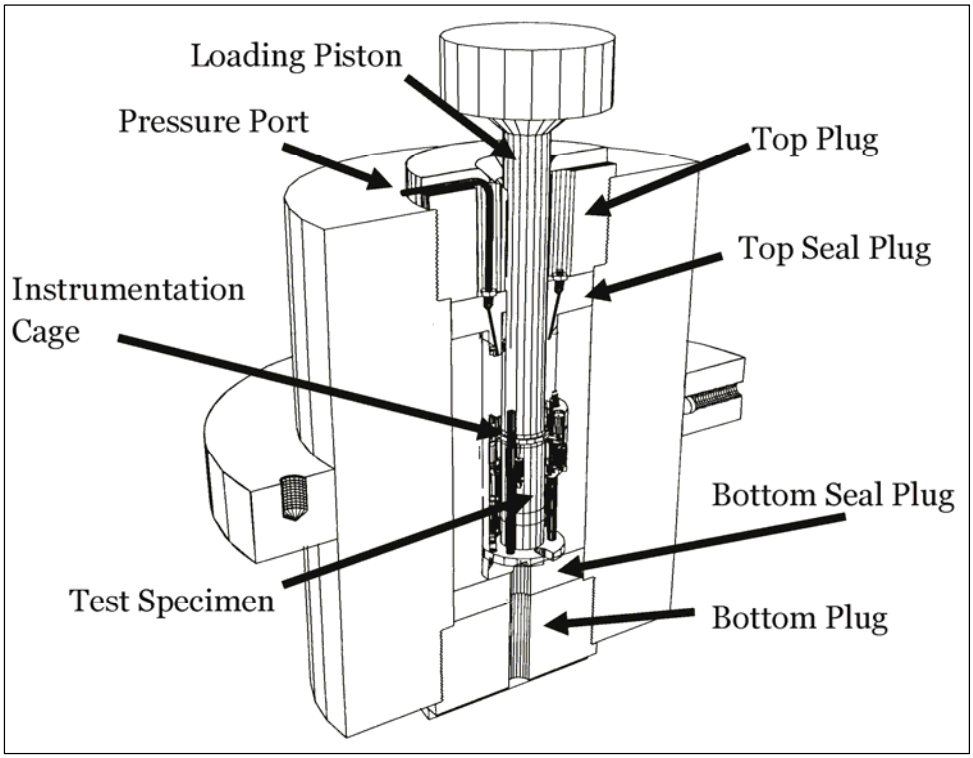

Figure 2. 600 MPa pressure vessel details.

Confining pressure was measured outside the vessel by a transducer mounted in the confining fluid line.

Outputs from the various instruments were electronically amplified and filtered, and the conditioned signals were recorded by computer-controlled, 16-bit, analog-to-digital converters. The data acquisition systems sampled the data channels every 1 to 5 sec, converted the measured voltages to engineering units, and stored the data for further processing.

Test instrumentation

The vertical deflection measurement system for all tests consisted of two linear variable differential transformers (LVDTs) mounted vertically on the instrumentation stands and positioned 180 deg apart. They were oriented to measure the displacement between the top and base caps, thus, providing a measure of the axial deformations of the specimen. A linear potentiometer was mounted external to the pressure vessel so as to measure the displacement of the piston through which axial loads were applied. This provided a backup to the vertical LVDTs in the event they exceeded their calibrated range.

Two types of radial deflection measurement systems (lateral deformeters) were used in this test program. The output of each was calibrated to the radial displacement of the two footings that were glued to the sides of the test specimen (Figure 1). These two small, steel footings were mounted 180 deg apart at the specimen's mid-height. The footing faces were machined to match the curvature of the test specimen. A threaded post extended from the outside of each footing and protruded through the membrane. The footings were mounted to the specimen prior to placement of the membrane. Once the membranes were in place, steel caps were screwed onto the threaded posts to seal the membrane to the footing. The lateral deformeter ring was attached to these steel caps with set-screws. The completed specimen lateral deformeter setup is shown in Figure 3.

One type of lateral deformeter consisted of an LVDT mounted on a hinged ring; the LVDT measured the expansion or contraction of the ring. This lateral deformeter was used over smaller ranges of radial deformation when the greatest measurement accuracy was required. This lateral deformeter was used for the UX tests. This design is similar to the radial-deformeter design provided by Bishop and Henkel (1962). When the specimen expanded (or contracted), the hinged deformeter ring opened (or closed), causing a change in the electrical output of the horizontally mounted LVDT.

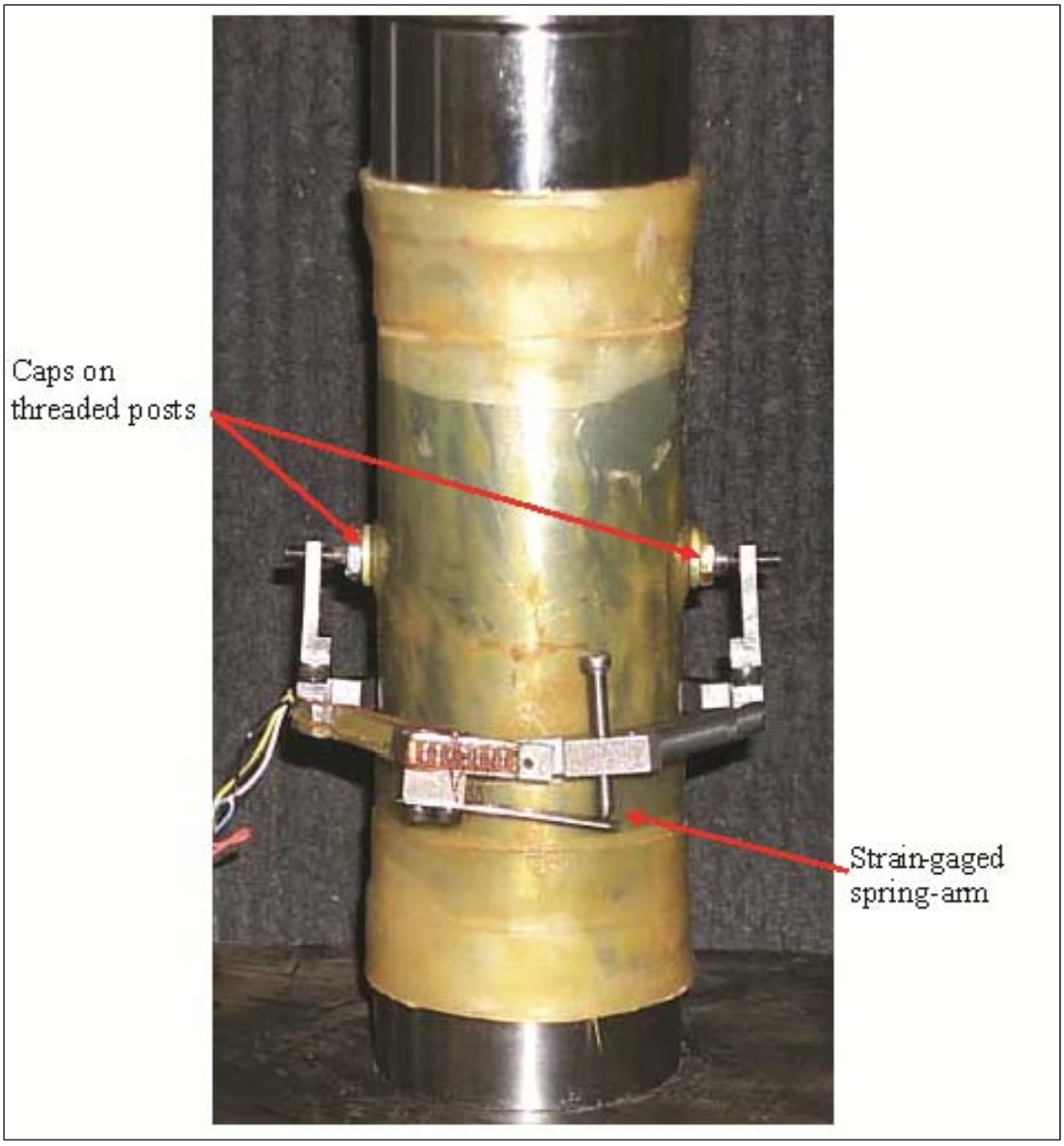

Figure 3. Spring-arm lateral deformeter mounted on test specimen.

The second type of lateral deformeter, which was used for the TXC tests, consisted of two strain-gaged spring-steel arms mounted on a double-hinged ring; the strain-gaged arms deflected as the ring expanded or contracted. This lateral deformeter was used when the greatest radial deformation range was required and, therefore, was less accurate than the LVDT deformeter. With this deformeter, when the specimen expanded or contracted, the rigid deformeter ring flexed about its hinge, causing a change in the electrical output of the strain-gaged spring-arm. The output of the spring-arms was calibrated to the specimen's radial deformation.

Test descriptions

The TXC tests were conducted in two phases. During the first, the hydrostatic compression phase, the cylindrical test specimen was subjected to an increase in hydrostatic pressure while measurements of the specimen's height and diameter changes were made. The data typically are plotted as pressure versus volumetric strain, the slope of which, assuming elastic theory, is the bulk modulus, K. The second phase of the TXC test, the shear phase, was conducted after the desired confining pressure was applied during the HC phase. While holding the desired confining pressure constant, axial load was increased, and measurements of the changes in the specimen's height and diameter were made. The axial (compressive) load was increased until the specimen failed. The shear data generally are plotted as principal stress difference versus axial strain, the slope of which represents Young's modulus, E. The maximum principal stress difference that a given specimen can support, or the principal stress difference at 15 percent axial strain during the shear loading, whichever occurs first, is defined as the peak strength.

A uniaxial strain (UX) test was conducted by applying axial load and confining pressure simultaneously so that, as the cylindrical specimen shortened, its diameter remained unchanged (i.e., zero radial strain boundary conditions were maintained). The data generally are plotted as axial stress versus axial strain, the slope of which is the constrained modulus, M. The data also are plotted as principal stress difference versus mean normal stress, the slope of which is twice the shear modulus, G, divided by the bulk modulus, K (i.e., $2G/K$, or, in terms of Poisson's ratio ν, $3(1-2\nu)/(1+\nu)$).

Definition of stresses and strains

During the mechanical property tests, measurements typically were made of the axial and radial deformations of the specimen as confining pressure and/or axial load was applied or removed. These measurements, along with the pre-test measurements of the initial height and diameter of the specimen, were used to convert the measured test data to true stresses and engineering strains.[2]

Axial strain, ε_a, was computed by dividing the measured axial deformation, Δh (change in height), by the original height h_o, i.e., $\varepsilon_a = \Delta h / h_o$. Similarly,

[2] Compressive stresses and strains are positive in this report.

radial strain, ε_r, was computed by dividing the measured radial deformation, Δd (change in diameter), by the original diameter d_o (i.e., $\varepsilon_r = \Delta d/d_o$). For this report, volumetric strain was assumed to be the sum of the axial strain and twice the radial strain, $\varepsilon_v = \varepsilon_a + 2\varepsilon_r$.

The principal stress difference, q, was calculated by dividing the axial load by the cross-sectional area of the specimen, A, which is equal to the original cross-sectional area, A_o, multiplied by $(1 - \varepsilon_r)^2$. In equation form,

$$q = (\sigma_a - \sigma_r) = \frac{\text{Axial Load}}{\text{A}_\text{o}(1-\varepsilon_r)^2} \quad (1)$$

where σ_a is the axial stress and σ_r is the radial stress. The axial stress is related to the confining pressure and the principal stress difference by

$$\sigma_a = q + \sigma_r \quad (2)$$

The mean normal stress, p, is the average of the applied principal stresses. In cylindrical geometry,

$$p = \frac{(\sigma_a + 2\sigma_r)}{3} \quad (3)$$

Results

Results from all of the mechanical property tests conducted on cylindrical specimens are presented in Plates 1 through 14 in Appendix A. One data plate is presented for each test with reliable results. Each plate for the TXC and UX tests displays four plots: (a) principal stress difference versus mean normal stress, (b) principal stress difference versus axial strain, (c) volumetric strain versus mean normal stress, and (d) volumetric strain versus axial strain.

3 Analysis of Test Results

Introduction

An analysis of the results from laboratory tests conducted on cylindrical specimens of adobe is presented in this chapter. The purpose of this investigation was to characterize the strength and constitutive properties of the material. As described in Chapter 2, 14 successful mechanical property tests were conducted on cylindrical specimens in this investigation. The analysis in this chapter is based on the results from 12 TXC tests and two UX tests.

Hydrostatic compression test results

Undrained compressibility data were obtained during the hydrostatic loading phases of the 12 TXC tests. The pressure-volume data from selected HC phases are plotted in Figure 4. A review of the composition properties for these six test specimens in Table 1, especially their values of initial dry density, indicates that HC compressibility is slightly affected by initial dry density (i.e., increased compressibility with decreased dry density). Figure 5 presents the pressure-time histories for the HC phases of the TXC tests. During the HC phases of the TXC tests, the pressure was intentionally held constant for a period of time prior to the shear phases. During each hold in pressure, the volumetric strains continued to increase, which indicates that adobe is susceptible to creep (Figures 4 and 5). Based on the data from the hydrostatic loadings from TXC tests in Figure 4, the initial elastic bulk modulus for adobe is approximately 169 MPa.

Triaxial compression test results

Shear and failure data were successfully obtained from 12 unconsolidated-undrained TXC tests. Recall from Chapter 2 that the second phase of the TXC test, the shear phase, was conducted after the desired confining pressure was applied during the HC phase. Results from the TXC tests are plotted in Figures 6 through 23. In all the figures, the axial and volumetric strains at the beginning of the shear phase were set to zero (i.e., only the strains during shear are plotted).

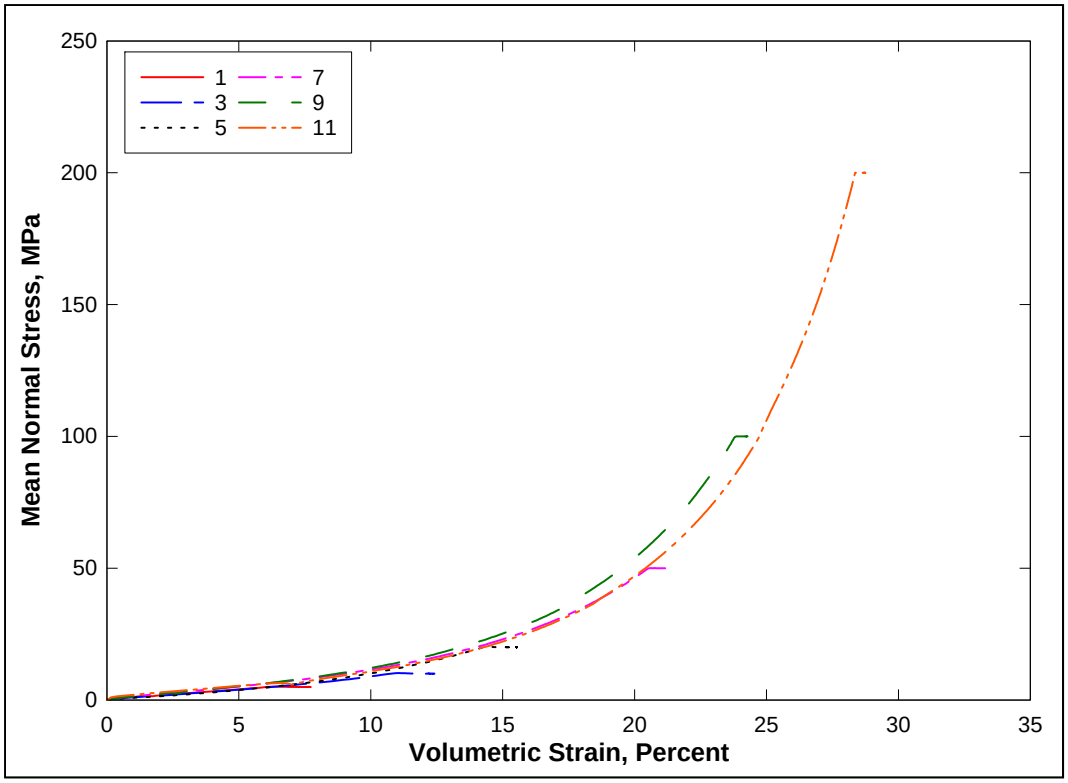

Figure 4. Pressure-volume responses from the HC phase of selected TXC tests.

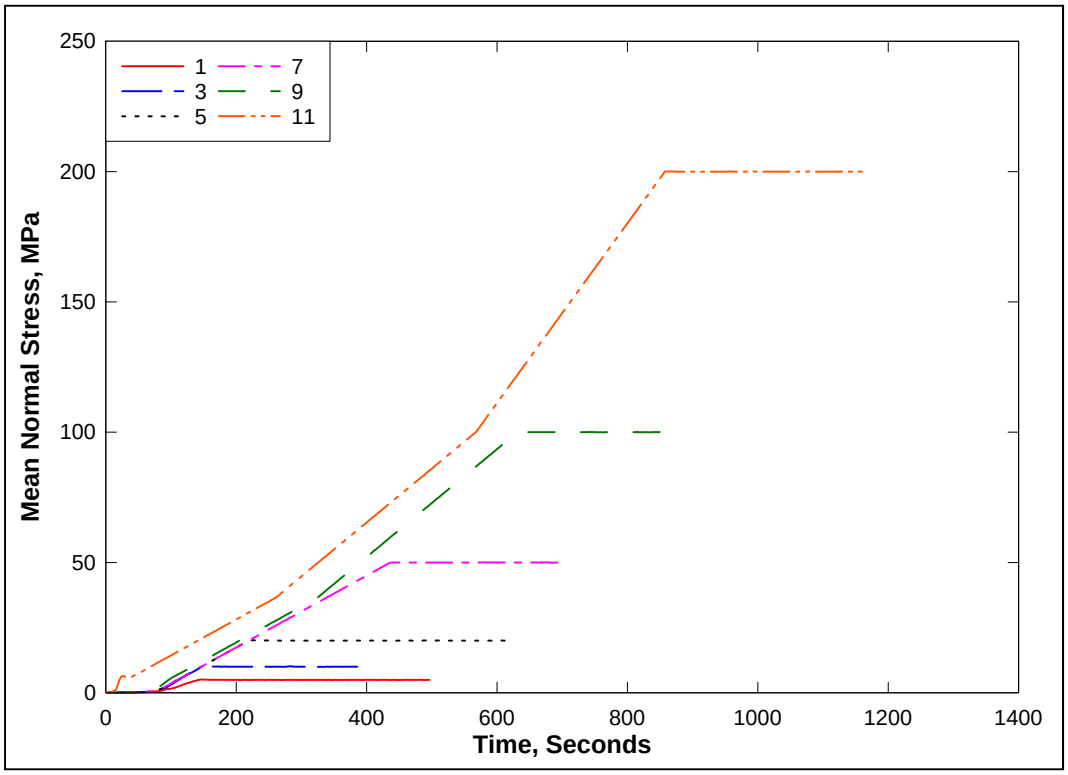

Figure 5. Pressure-time histories from the HC phase of selected TXC tests.

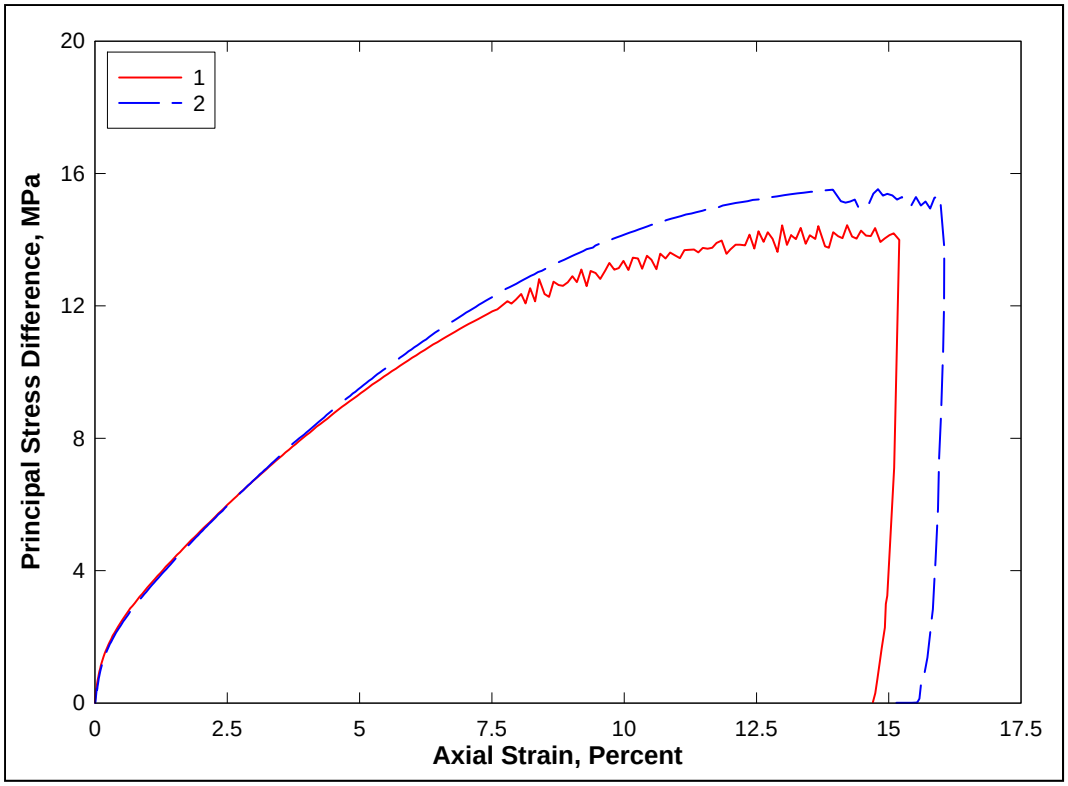

Figure 6. Stress-strain curves from TXC tests at a confining pressure of 5 MPa.

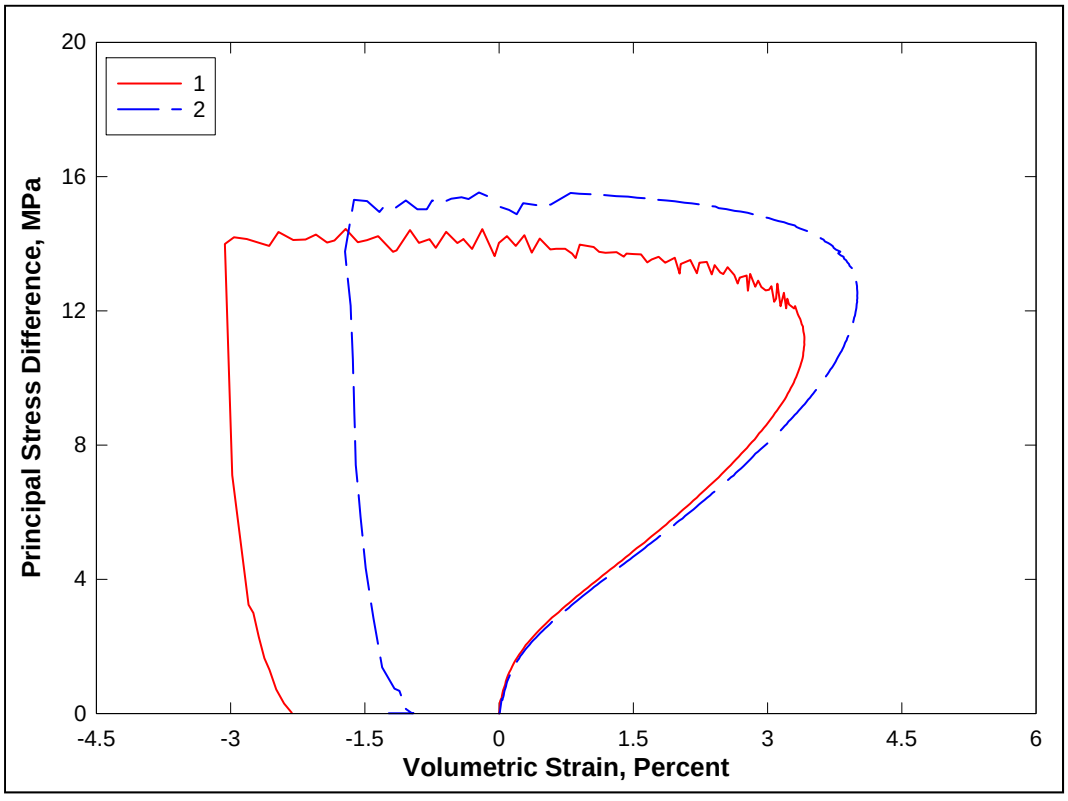

Figure 7. Stress difference-volumetric strain during shear from TXC tests at a confining pressure of 5 MPa.

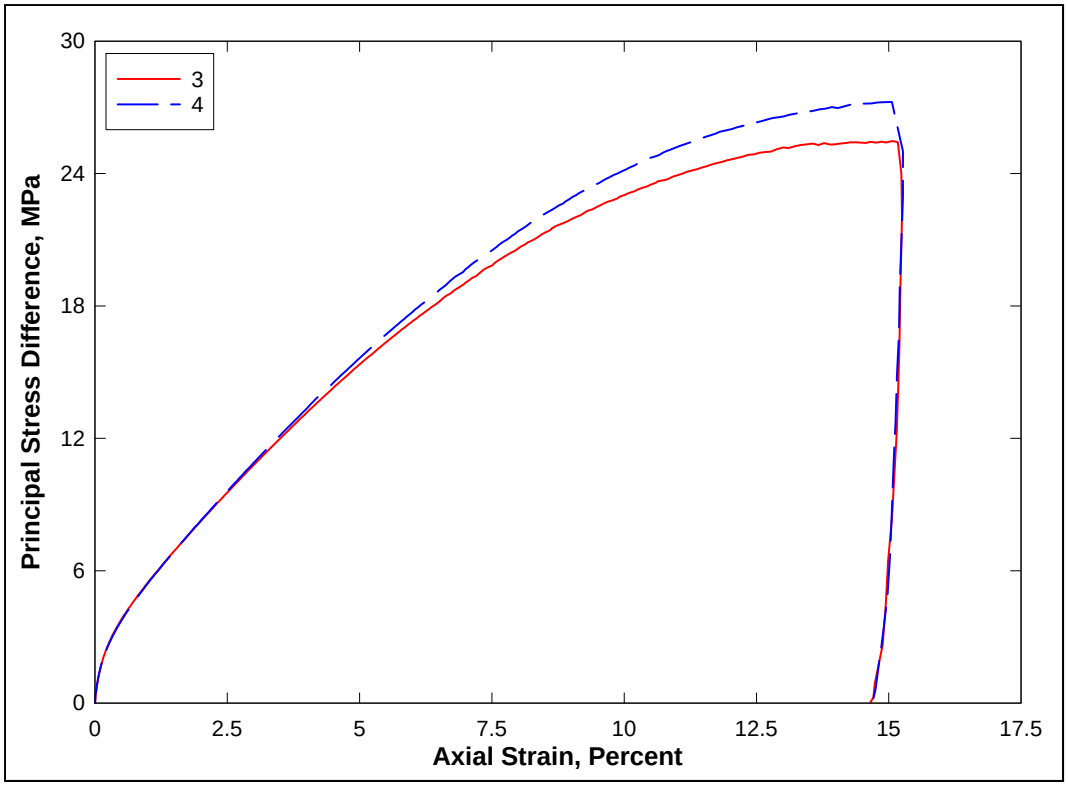

Figure 8. Stress-strain curves from TXC tests at a confining pressure of 10 MPa.

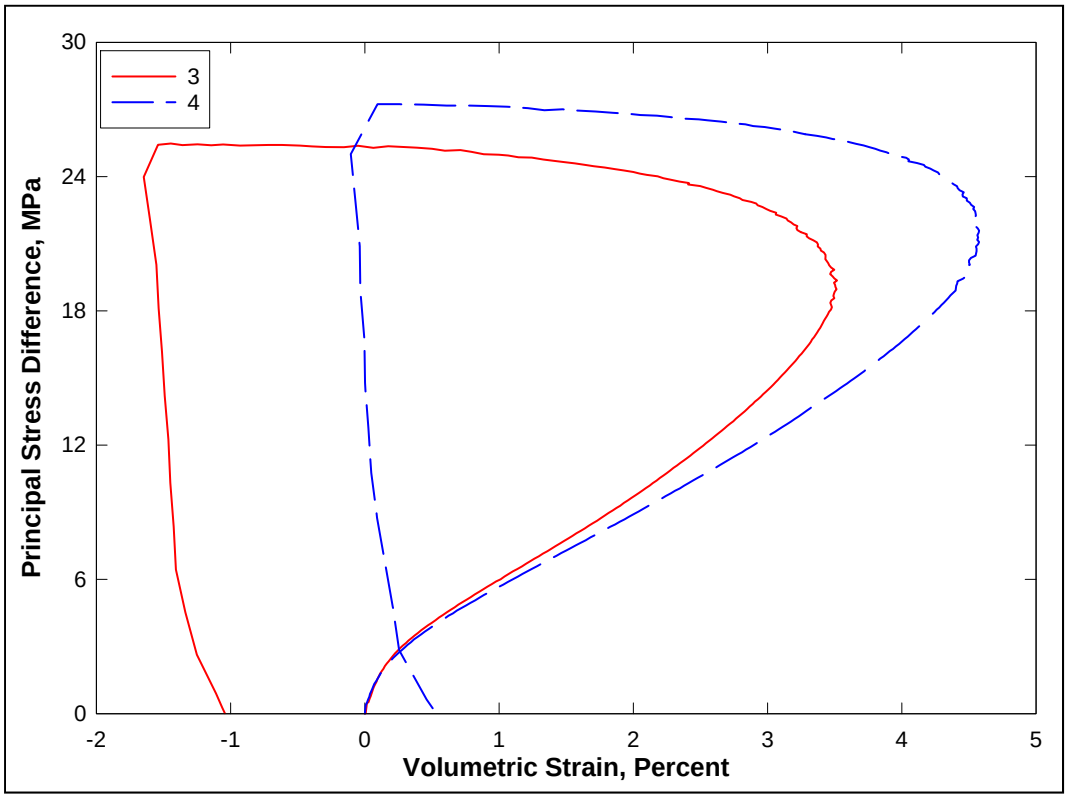

Figure 9. Stress difference-volumetric strain during shear from TXC tests at a confining pressure of 10 MPa.

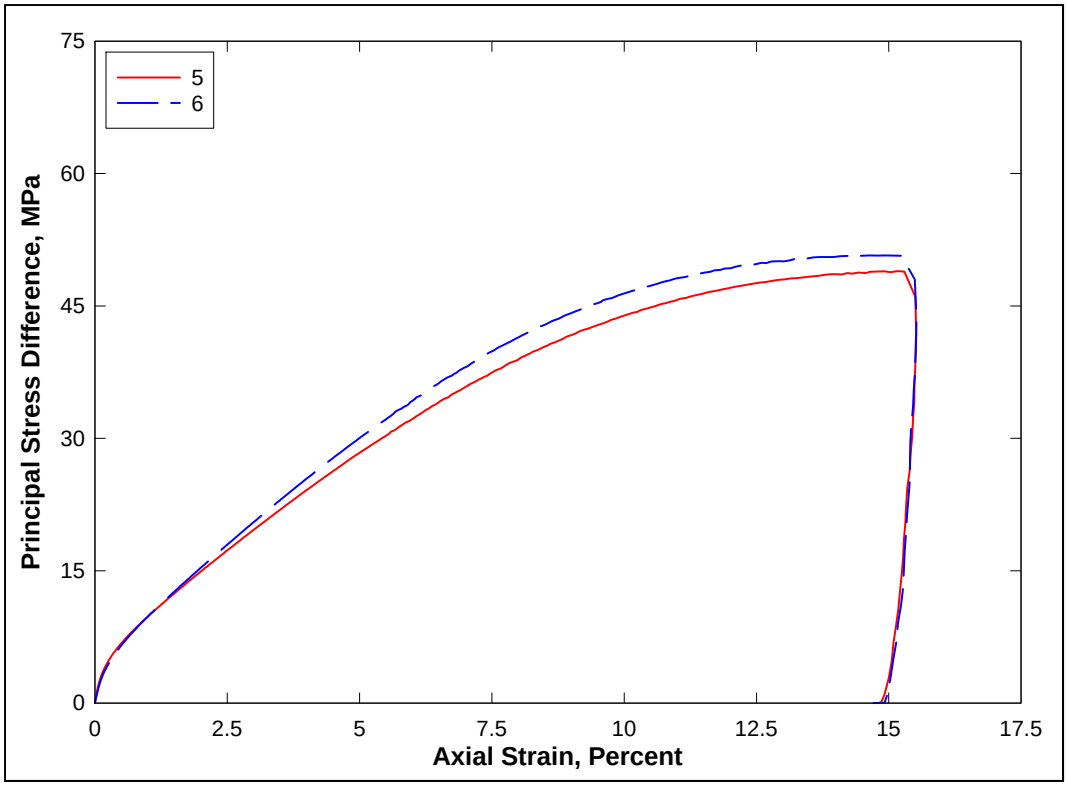

Figure 10. Stress-strain curves from TXC tests at a confining pressure of 20 MPa.

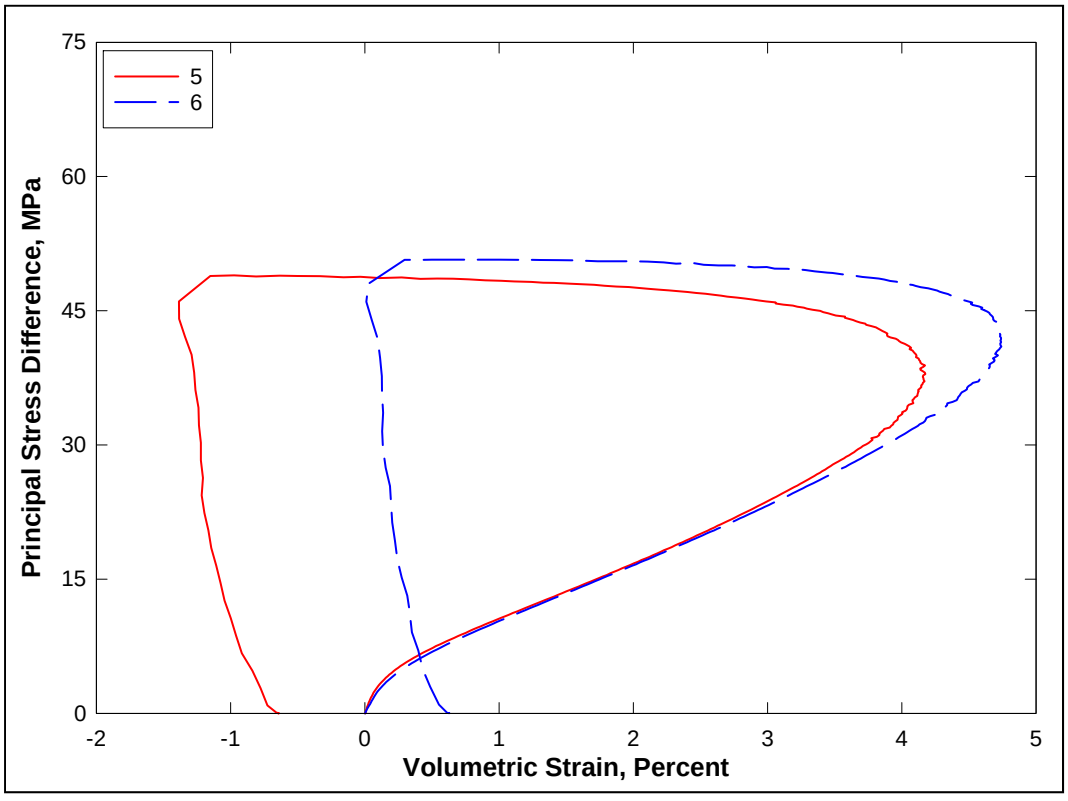

Figure 11. Stress difference-volumetric strain during shear from TXC tests at a confining pressure of 20 MPa.

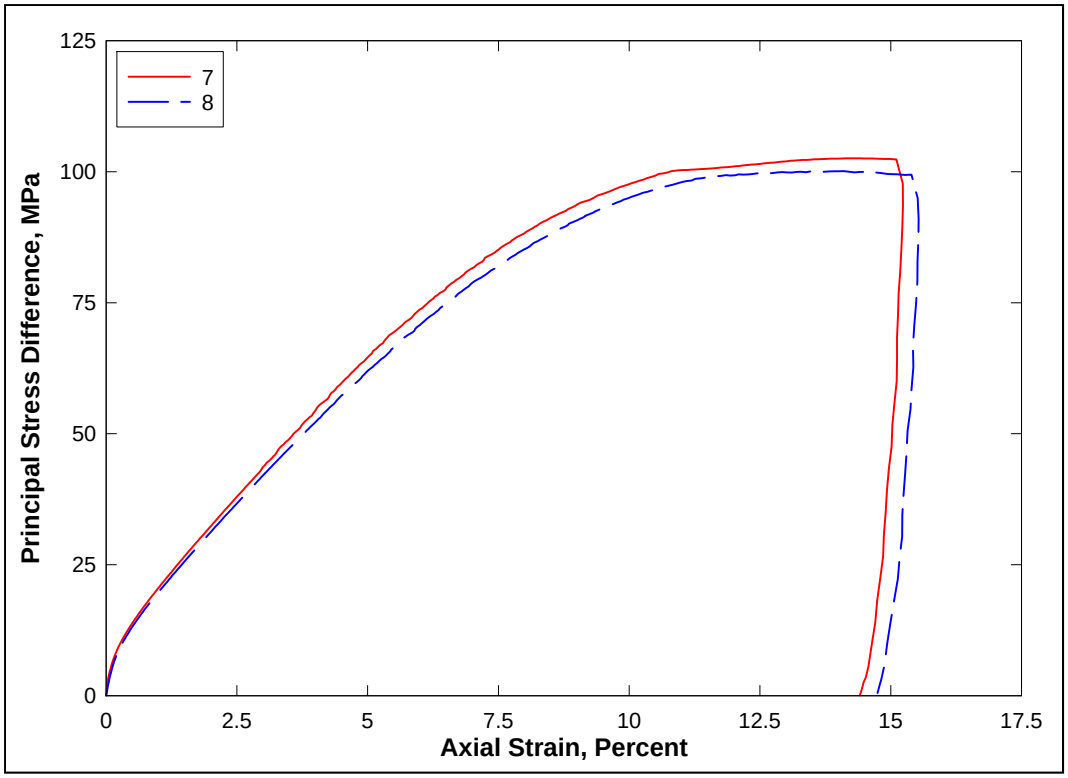

Figure 12. Stress-strain curves from TXC tests at a confining pressure of 50 MPa.

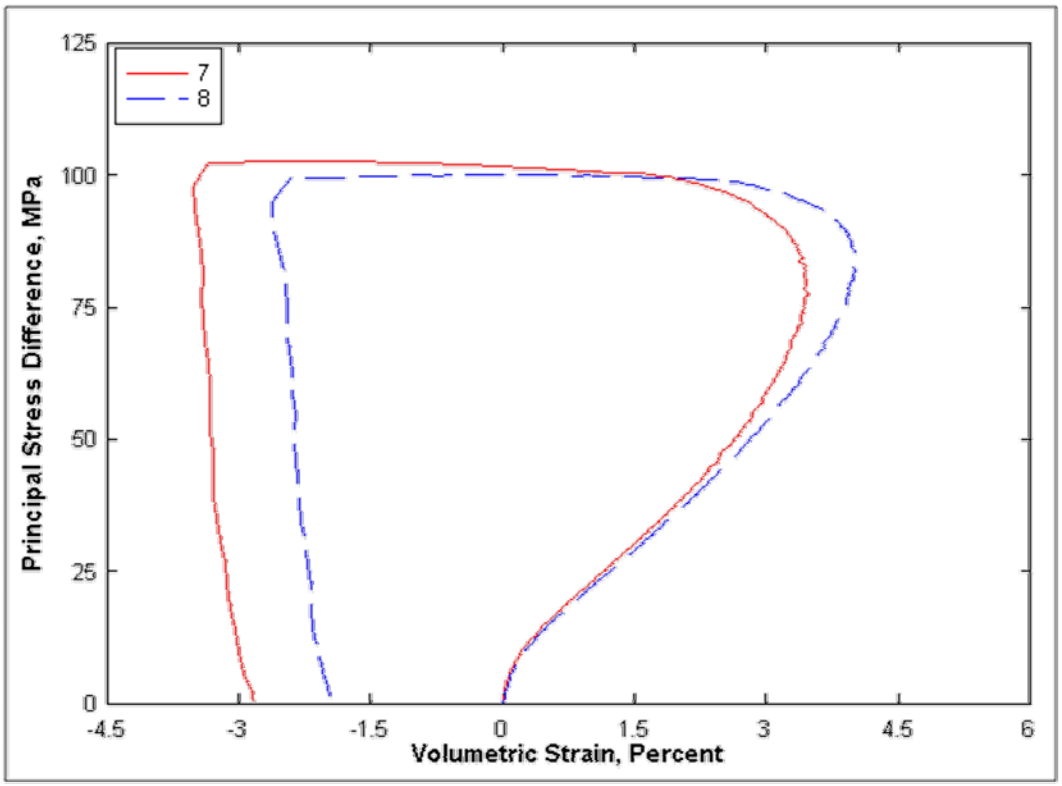

Figure 13. Stress difference-volumetric strain during shear from TXC tests at a confining pressure of 50 MPa.

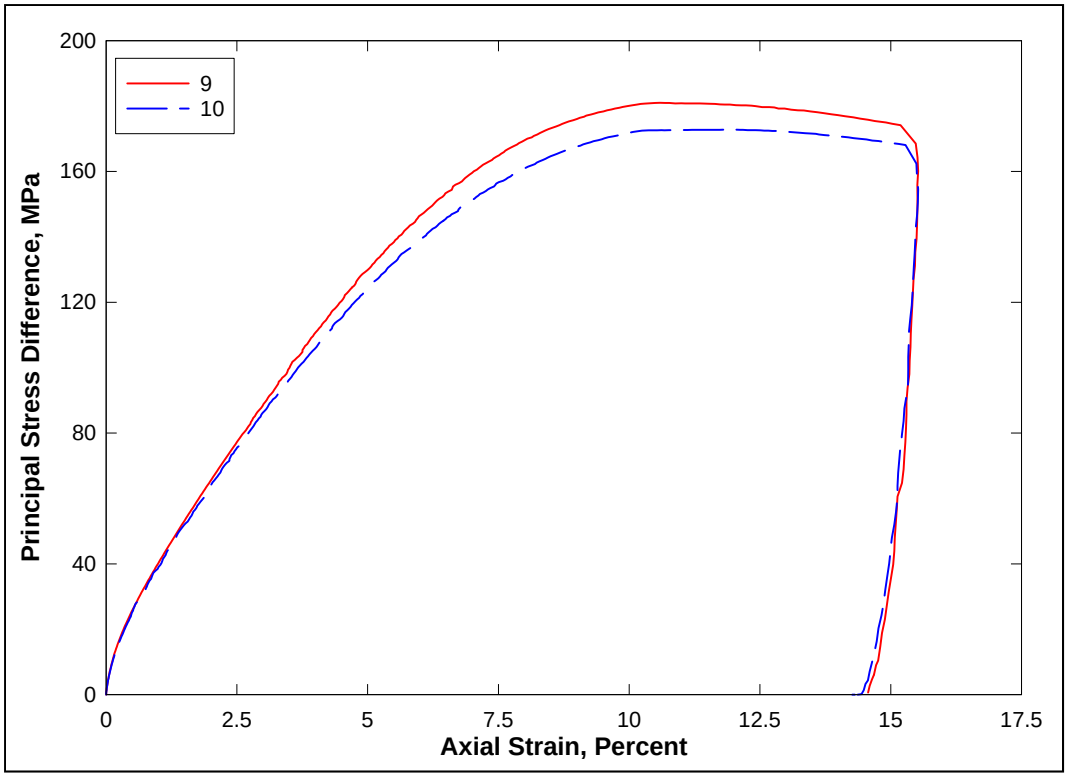

Figure 14. Stress-strain curves from TXC tests at a confining pressure of 100 MPa.

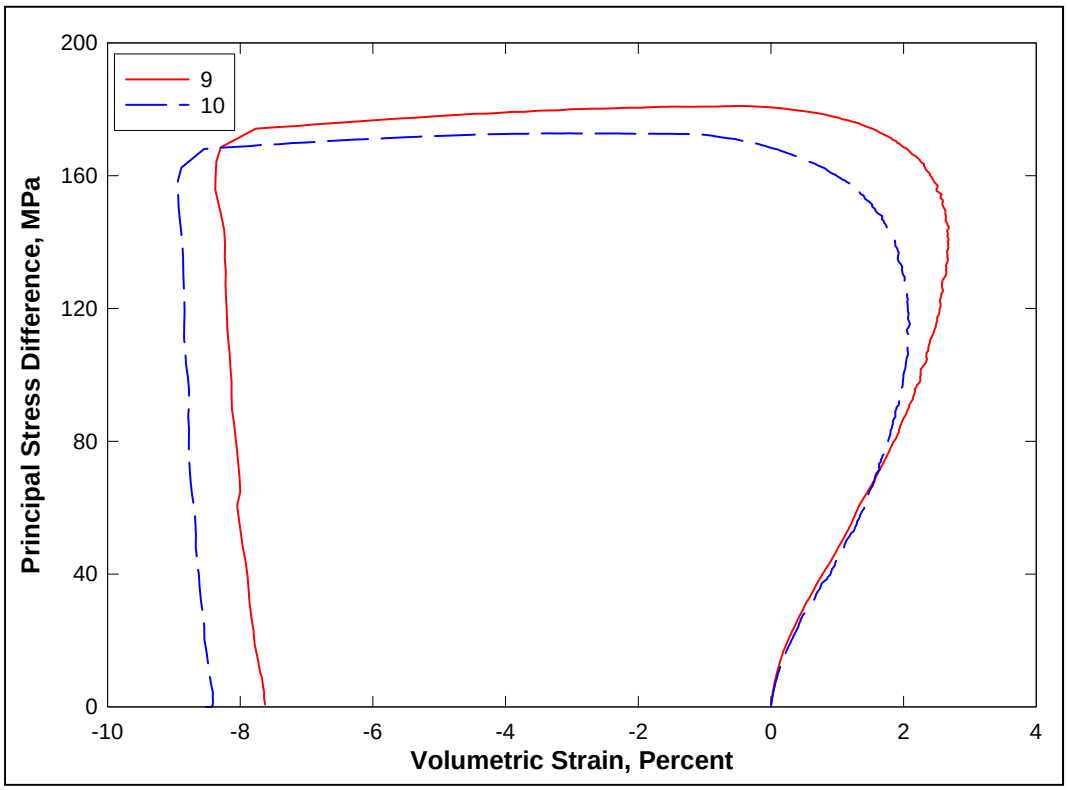

Figure 15. Stress difference-volumetric strain during shear from TXC tests at a confining pressure of 100 MPa.

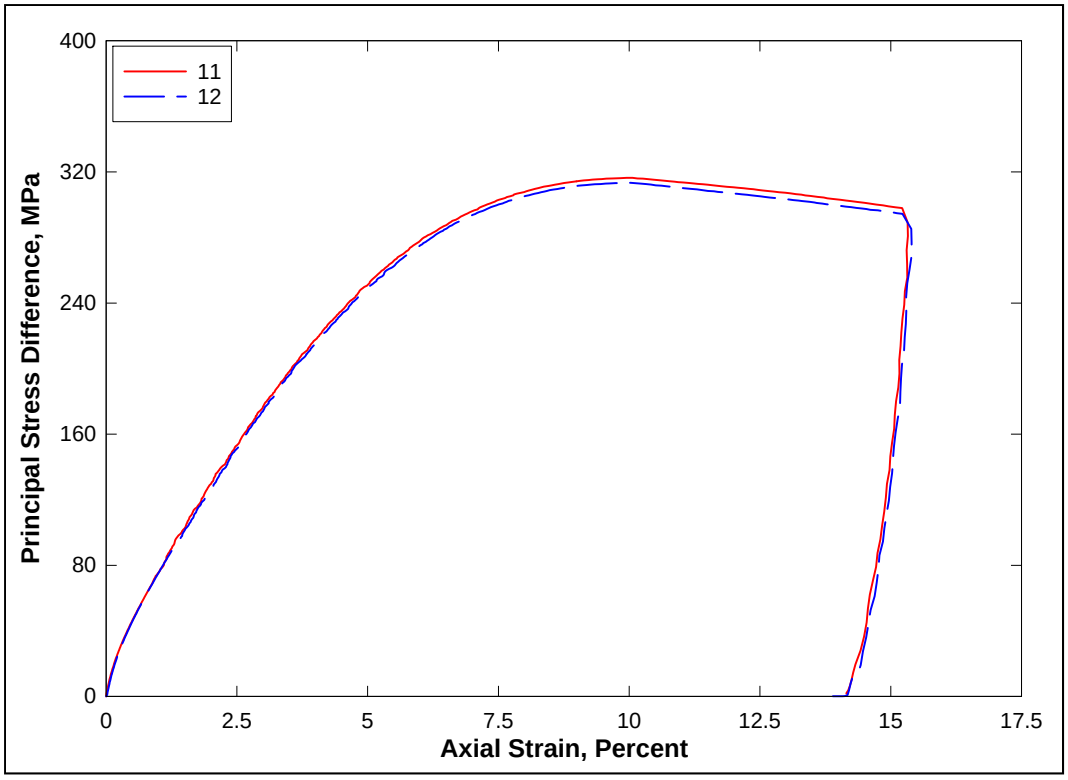

Figure 16. Stress-strain curves from TXC tests at a confining pressure of 200 MPa.

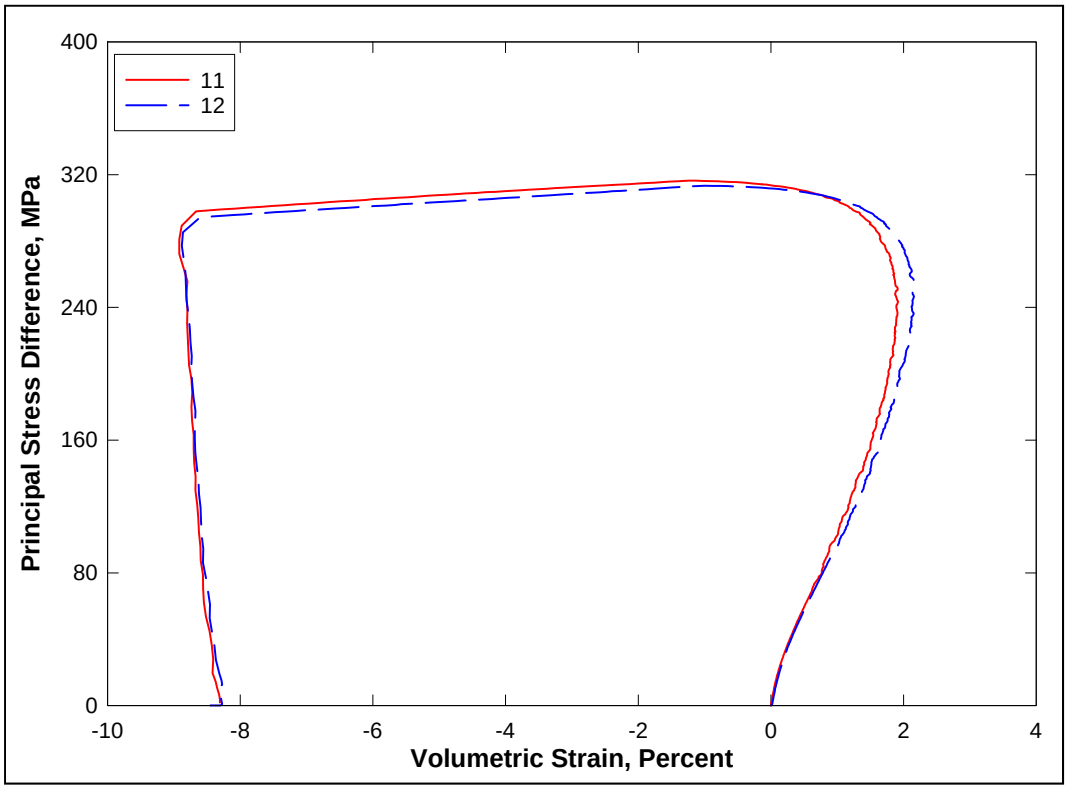

Figure 17. Stress difference-volumetric strain during shear from TXC tests at a confining pressure of 200 MPa.

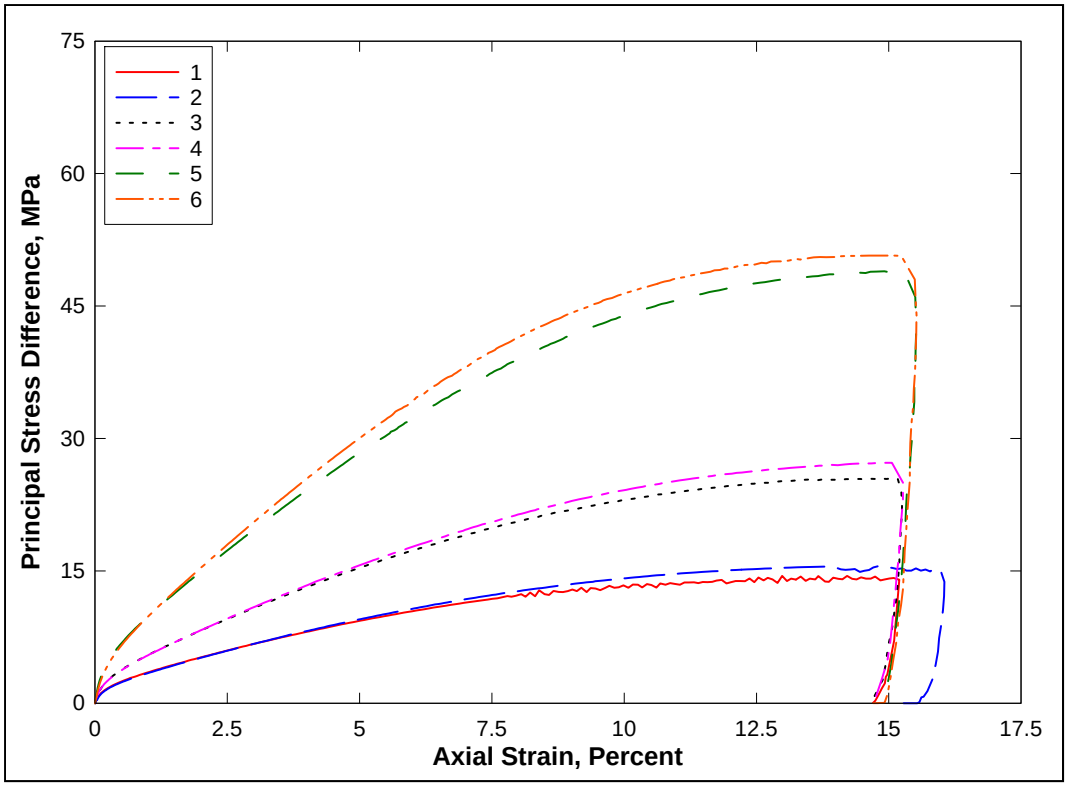

Figure 18. Stress-strain data from TXC tests at confining pressures between 5 and 20 MPa.

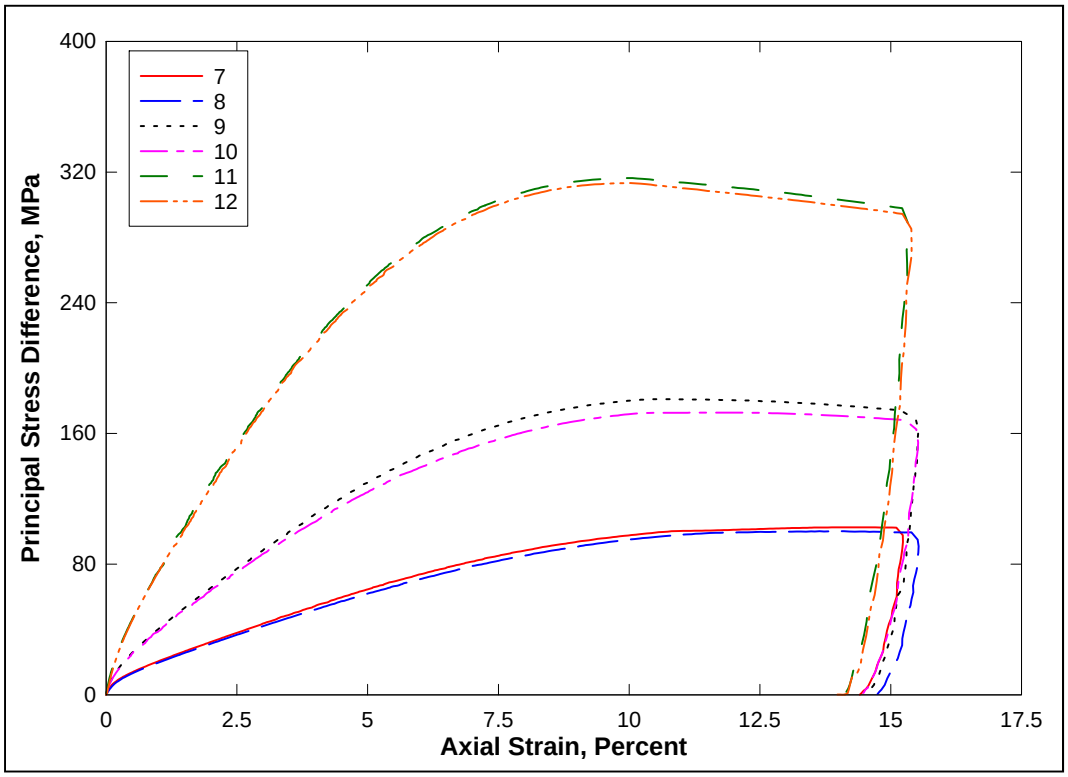

Figure 19. Stress-strain data from TXC tests at confining pressures between 50 and 200 MPa.

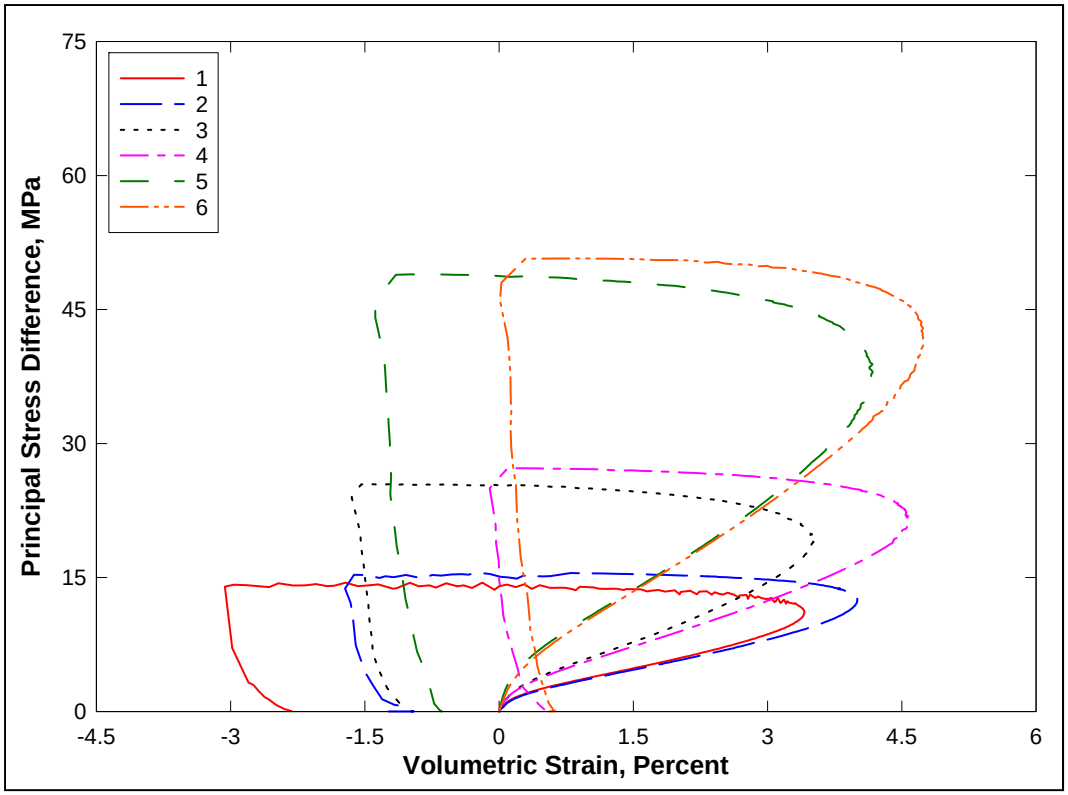

Figure 20. Stress difference-volumetric strain during shear from TXC tests at confining pressures between 5 and 20 MPa.

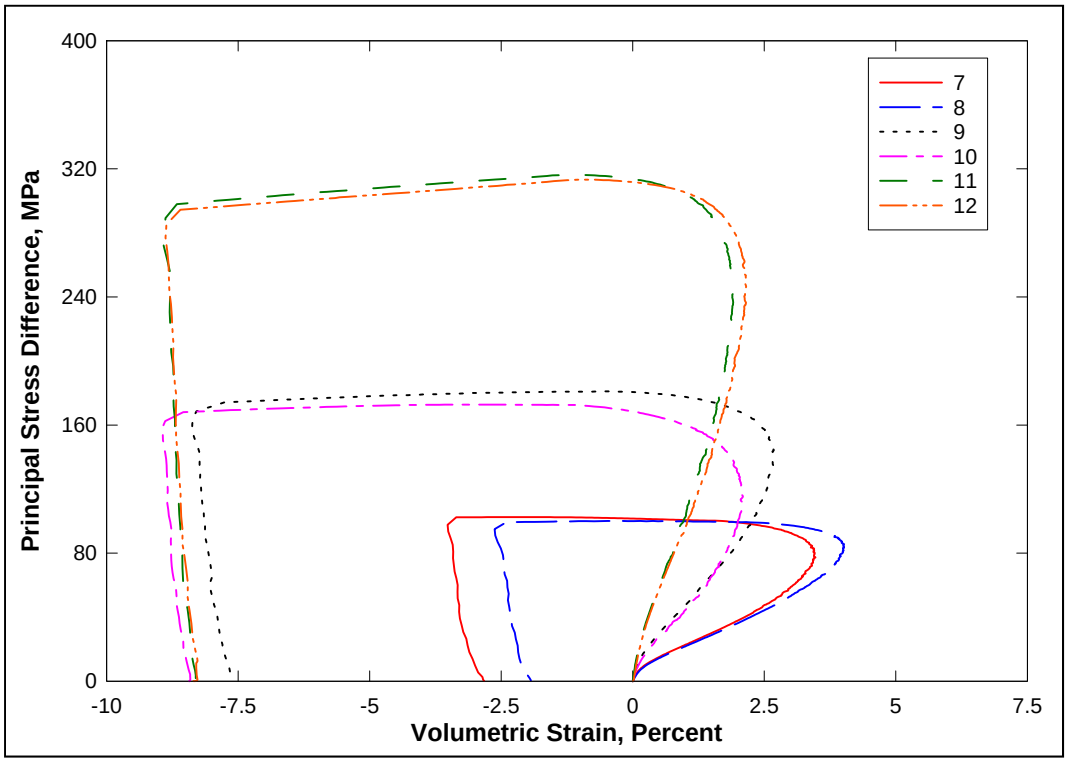

Figure 21. Stress difference-volumetric strain during shear from TXC tests at confining pressures between 50 and 200 MPa.

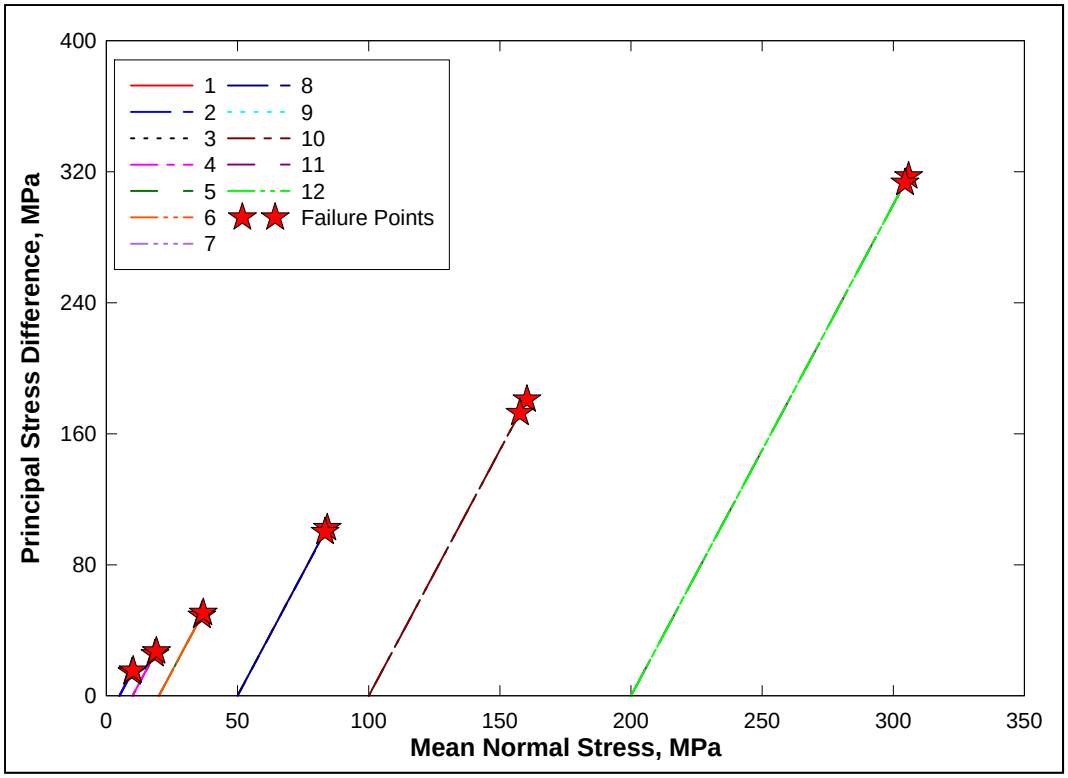

Figure 22. Shear failure data from TXC tests at confining pressures between 5 and 200 MPa.

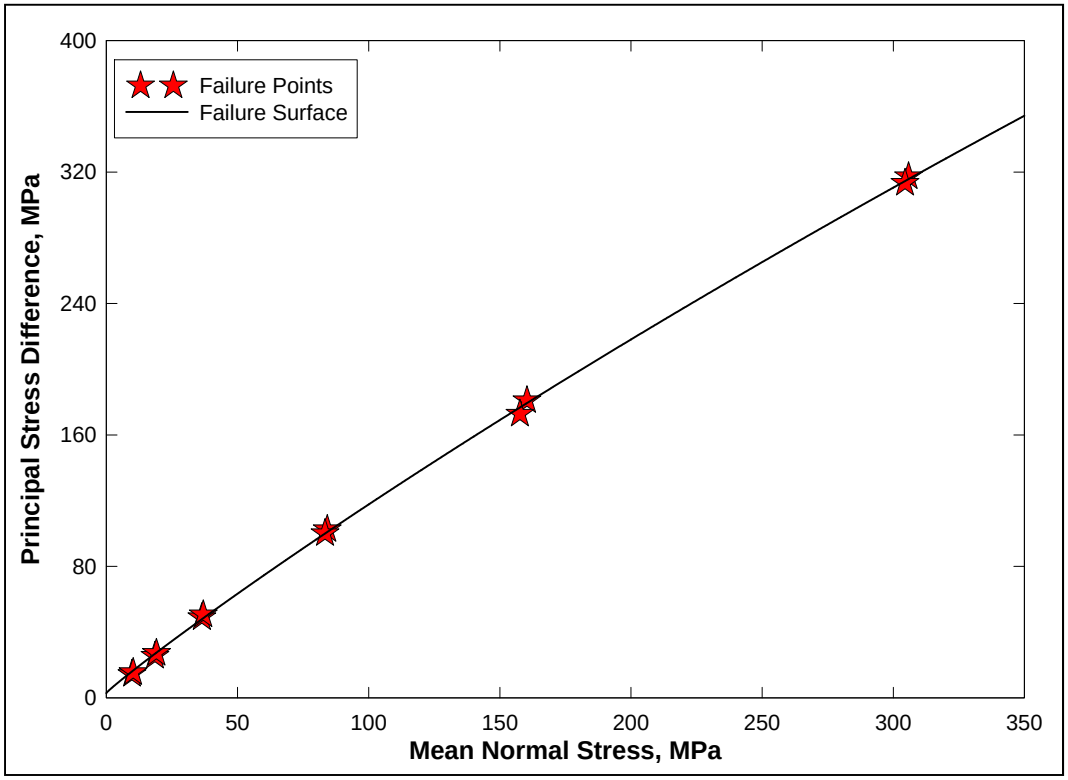

Figure 23. Failure data from TXC tests and recommended failure surface.

The TXC results are plotted as principal stress difference versus axial strain during shear and as principal stress difference versus volumetric strain during shear. The results are very consistent considering the inherent variability of the initial wet and dry densities and water contents of the specimens. The wet densities of the specimens ranged from 1.713 to 1.842 Mg/m^3, the dry densities ranged from 1.694 to 1.823 Mg/m^3, and the water contents ranged from 0.92 percent to 1.20 percent.

One general comment should be made concerning the unloading results. The vertical deformeters went out of range at 11 percent axial strain, so an external deformeter with less resolution was used to measure axial displacement greater than 11 percent. As a result, the final unloading stress-strain responses at axial strains less than 11 percent are more reliable than those at strains greater than 11 percent.

Test results for TXC tests conducted at confining pressures of 5, 10, 20, 50, 100, and 200 MPa are shown in Figures 6-7, 8-9, 10-11, 12-13, 14-15, and 16-17, respectively. The qualitative responses at these six levels of confining pressure are essentially the same. The shear responses were predominantly ductile, and peak strength increased with increased levels of confining pressure. Test specimens at 50 to 200 MPa showed that, as confining pressures increased, the amount of compaction decreased and the amount of dilation increased. Test specimens at confining pressures of 5 to 20 MPa showed the opposite trend in that, as the confining pressures increased, the amount of compaction increased and dilation decreased.

For comparison purposes, stress-strain responses from the TXC tests at confining pressures equal to or less than 20 MPa are plotted in Figure 18, and the responses at confining pressures of 50 MPa and above are plotted in Figure 19. Data from the TXC tests in Figures 18 and 19 are plotted in Figures 20 and 21, respectively, as principal stress difference versus volumetric strain during shear. As displayed in Figures 18 and 19, the initial loading of the material stiffens as the confining pressure increases. The initial loading will continue to stiffen as the material approaches void closure, the point at which all of the specimen's air-porosity is removed. In Figure 20, the volumetric strain during shear increases with increasing confining pressure, while in Figure 21 the volumetric strain during shear decreases with confining pressure. The compaction volumetric strain decreases at the higher confining pressure levels are due to the stiffening of the HC pressure-volume response, as was shown in Figure 4.

The failure data from all of the TXC tests are plotted in Figure 22 as principal stress difference versus mean normal stress; one stress path at each confining stress also is plotted. In Figure 23, a recommended failure surface is plotted with the TXC failure points. The quality of the failure data is very good, and the data exhibit very little scatter. The failure data exhibit a continuous increase in maximum principal stress difference with increasing values of mean normal stress. The adobe did not reach void closure and full saturation at the tested levels of pressure. Many materials can continue to gain strength with increasing pressure until all of the air porosity in the material has been removed (i.e., when void closure is reached).

Uniaxial strain test results

One-dimensional compressibility data were obtained from two undrained uniaxial strain (UX) tests with lateral stress measurements. Data from the tests are plotted in Figures 24 through 26: the stress-strain data from the UX tests are plotted in Figure 24, the pressure-volume data in Figure 25, and the stress path data with the TXC failure surface in Figure 26. The UX responses in Figures 24 and 25 are initially very compressible due to the ability of adobe to compact significantly. Test specimen 13 had an initial dry density of 1.781 Mg/m^3, while specimen 14 had an initial dry density of 1.776 Mg/m^3, which again implies that initial dry density affects compressibility.

Neither of the volumetric strains during the loading of each test specimen reached its respective air voids content, which indicates that the specimens did not become fully saturated near the peak stress. An initial constrained modulus of 270 MPa was calculated from the UX stress-strain loading data from test specimens 13 and 14 (Figure 24). The UX stress path in Figure 26 implies an initial value of Poisson's ratio of about 0.31. Using the bulk modulus determined from the HC phase of the TXC tests (169 MPa), an initial shear modulus was calculated to be 75.8 MPa. The initial constrained modulus and the shear modulus can be used to calculate an initial value of Young's modulus of 198 MPa. Finally, the UX stress paths soften after the material begins to crush, causing the data in Figure 26 to plot below the failure surface.

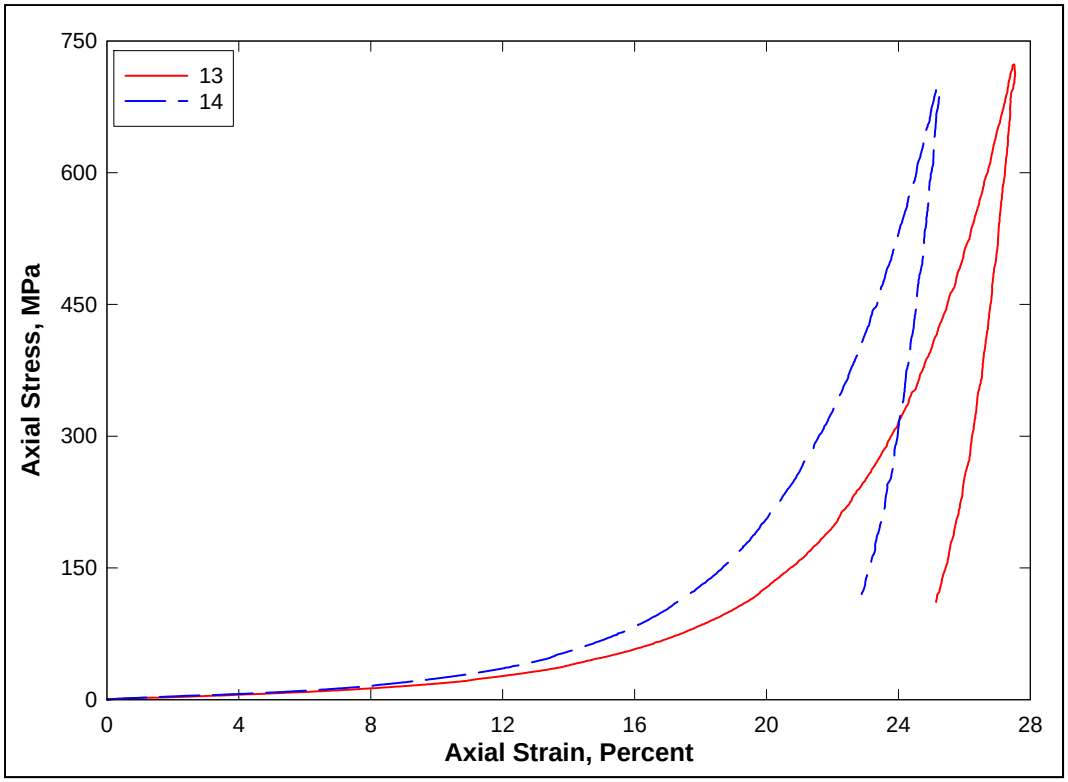

Figure 24. Stress-strain curves from UX tests.

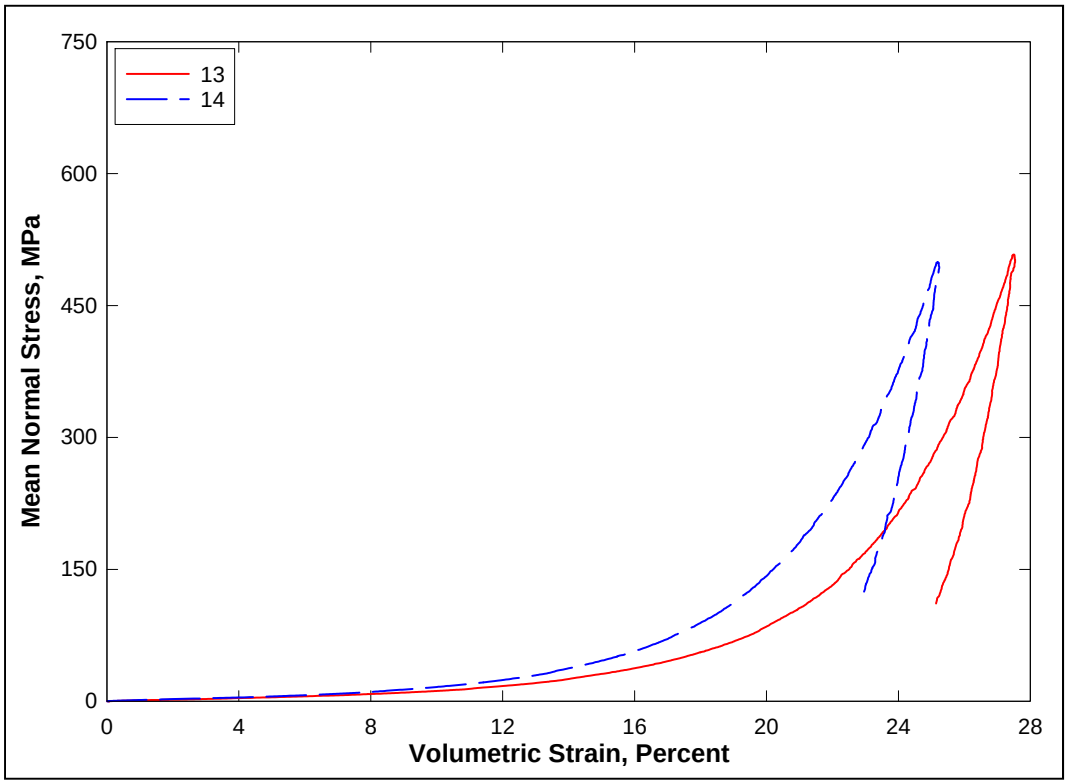

Figure 25. Pressure-volume data from UX tests.

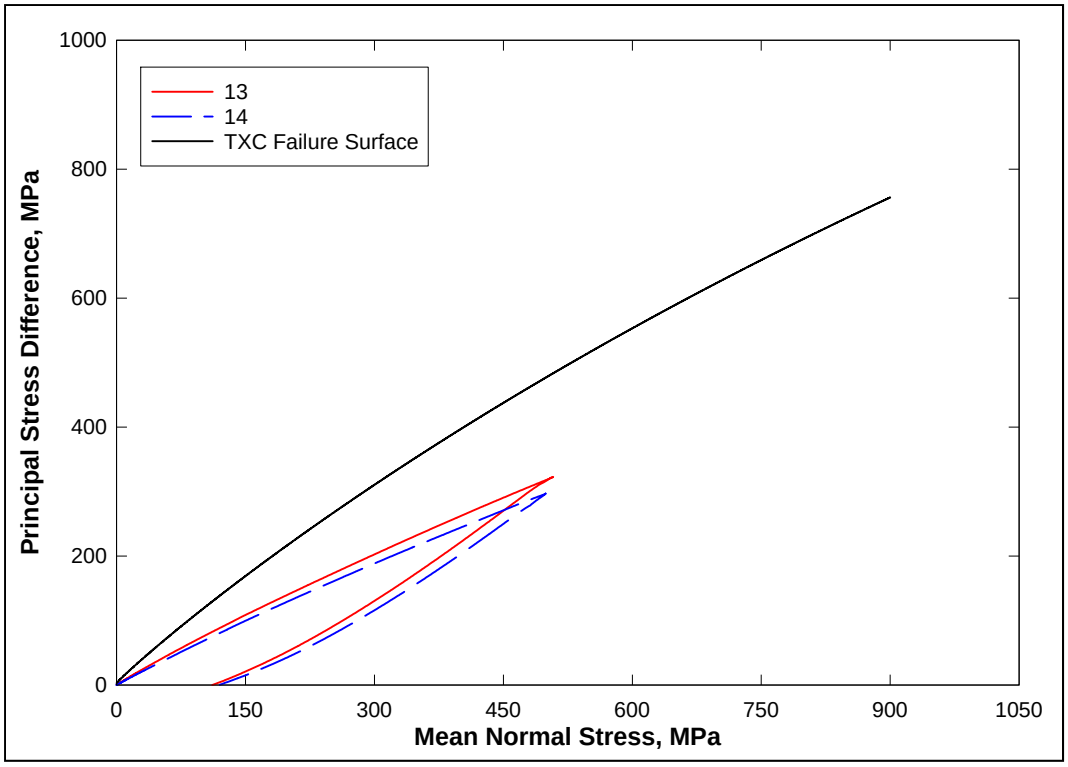

Figure 26. Stress paths from UX tests and failure surface from TXC tests.

4 Summary

Personnel in the Geotechnical and Structures Laboratory (GSL) at the U.S. Army Engineer Research and Development Center (ERDC) conducted a laboratory investigation to characterize the strength and constitutive property behavior of Scottsdale adobe. ERDC conducted 21 successful mechanical property tests, consisting of 12 triaxial compression tests, two uniaxial strain tests, and seven unconfined compression tests. In addition to the mechanical property tests, nondestructive pulse-velocity measurements were obtained on each specimen.

In general, the overall quality of the test data was good; limited scatter was observed in the data over repeated loading paths. Creep was observed during the HC phases of TXC tests. In addition, the HC phases of TXC tests and the UX compressibility data indicated that compressibility of the adobe was slightly dependent on initial dry density, in that specimens with higher initial dry density were less compressible. The TXC tests exhibited a continuous increase in maximum principal stress difference with increasing confining stress, and a well-defined compression failure surface was developed from these data at six levels of confining stress. At confining pressures at and below 20 MPa, the TXC tests exhibited increased compaction during early phases of shear loading with increased confining pressure but decreased dilation near peak strength. At confining pressures of 50 MPa to 200 MPa, the TXC tests exhibited opposite responses: decreased compaction during early shear loading with increases in confining pressure but increased dilation near peak strength. The compaction volumetric strain decreases at the higher levels of confining pressure were due to the stiffening of the HC volumetric responses.

References

American Society for Testing and Materials. 2009a. *Standard test method for pulse velocity through concrete*. Designation C 597-97. Philadelphia, PA: American Society for Testing and Materials.

_____. 2009b. *Standard test method for laboratory determination of water (moisture) content of soil and rock by mass*. Designation D 2216-98. Philadelphia, PA: American Society for Testing and Materials.

_____. 2009c. *Standard test method for preparing rock core specimens and determining dimensional and shape tolerances*. Designation D 4543-01. Philadelphia, PA: American Society for Testing and Materials.

Bishop, A. W. and D. J. Henkel. 1962. *The measurement of soil properties in the triaxial test*. London: Edward Arnold, Ltd.

Appendix A: Results from All of the Mechanical Property Tests Conducted on Cylindrical Specimens (Plates 1-14)

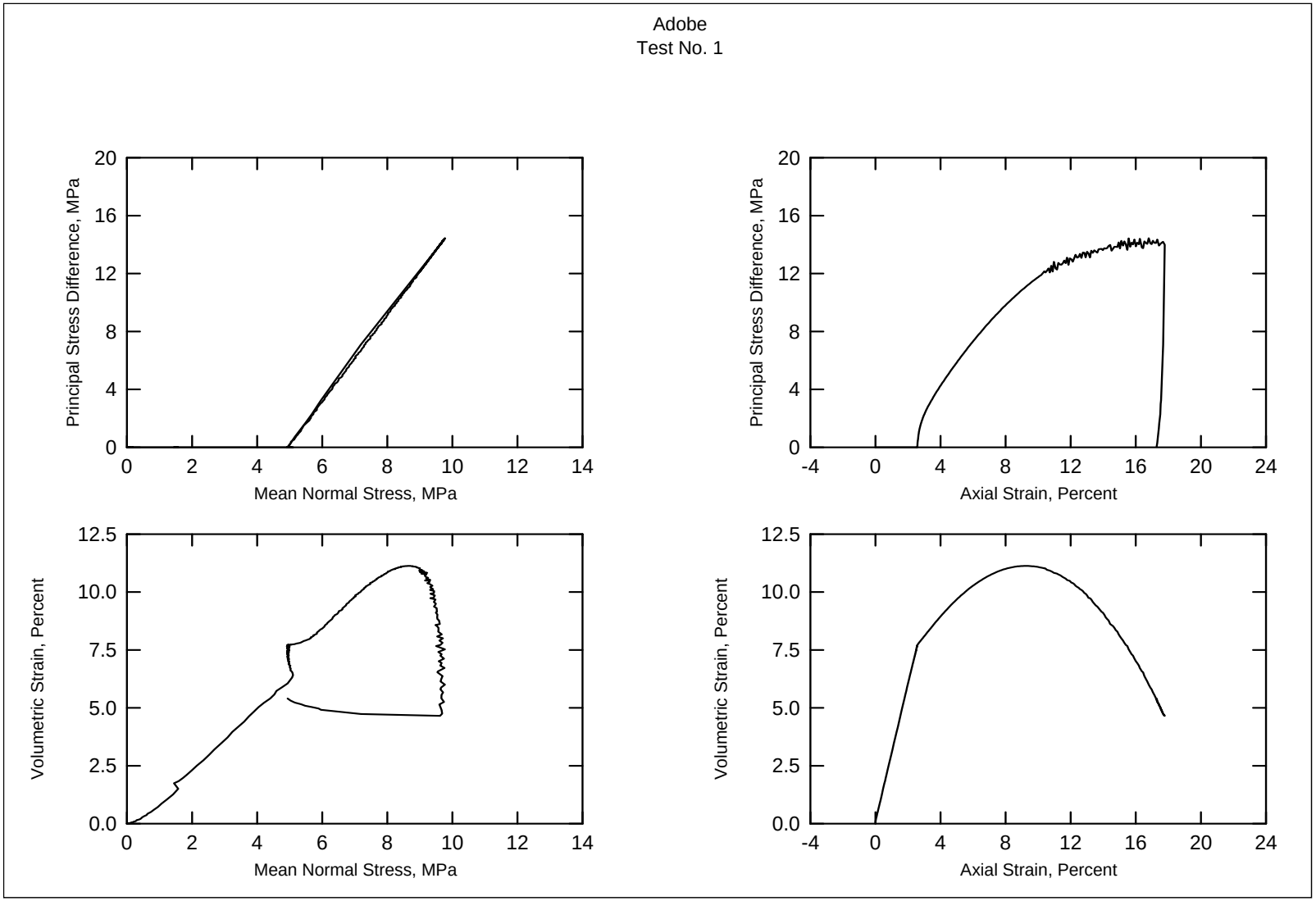
Adobe
Test No. 1
Principal Stress Difference, MPa
Mean Normal Stress, MPa
Principal Stress Difference, MPa
Axial Strain, Percent
Volumetric Strain, Percent
Mean Normal Stress, MPa
Volumetric Strain, Percent
Axial Strain, Percent

Plate 1

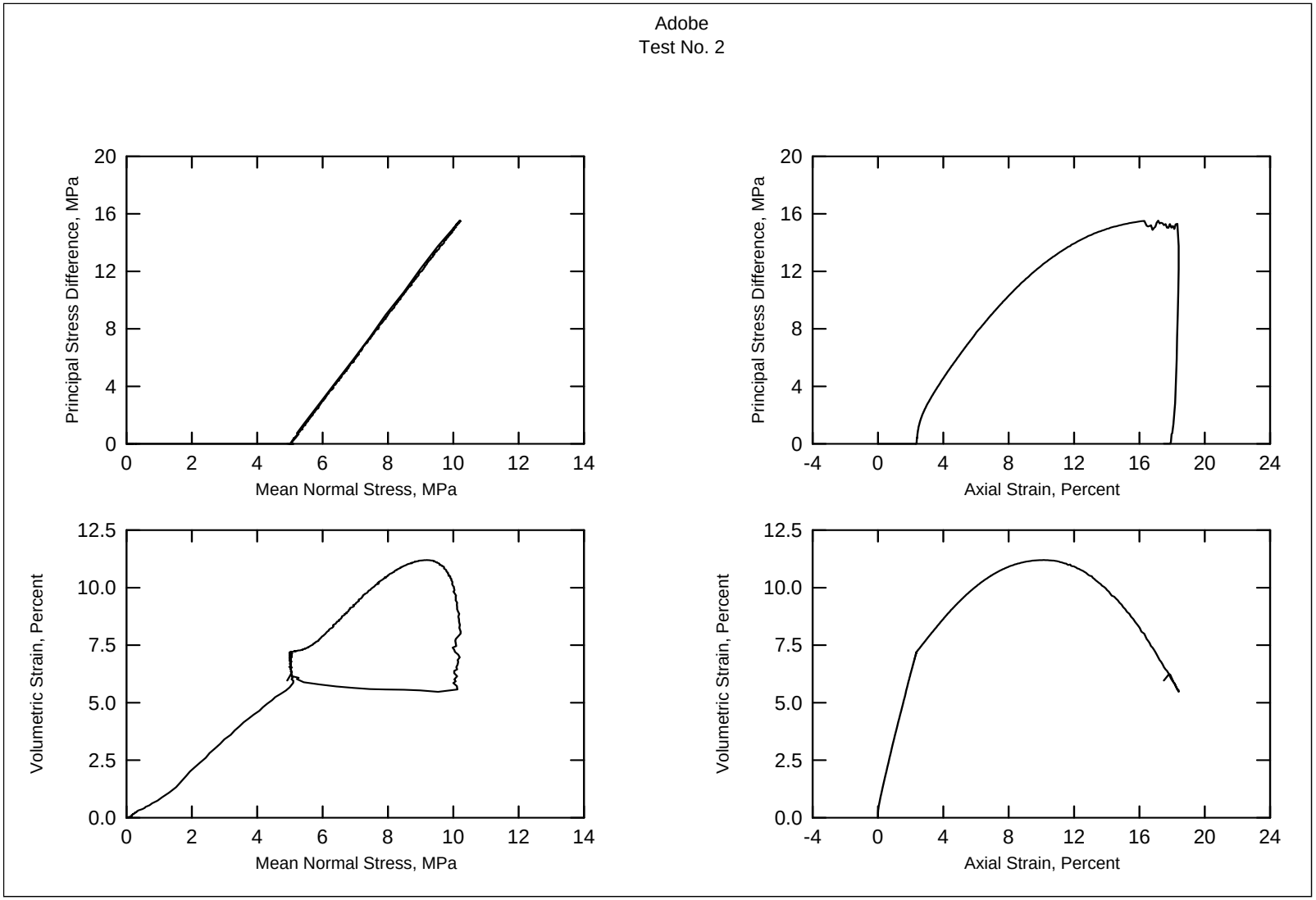
Adobe
Test No. 2
Principal Stress Difference, MPa
Mean Normal Stress, MPa
Principal Stress Difference, MPa
Axial Strain, Percent
Volumetric Strain, Percent
Mean Normal Stress, MPa
Volumetric Strain, Percent
Axial Strain, Percent

Plate 2

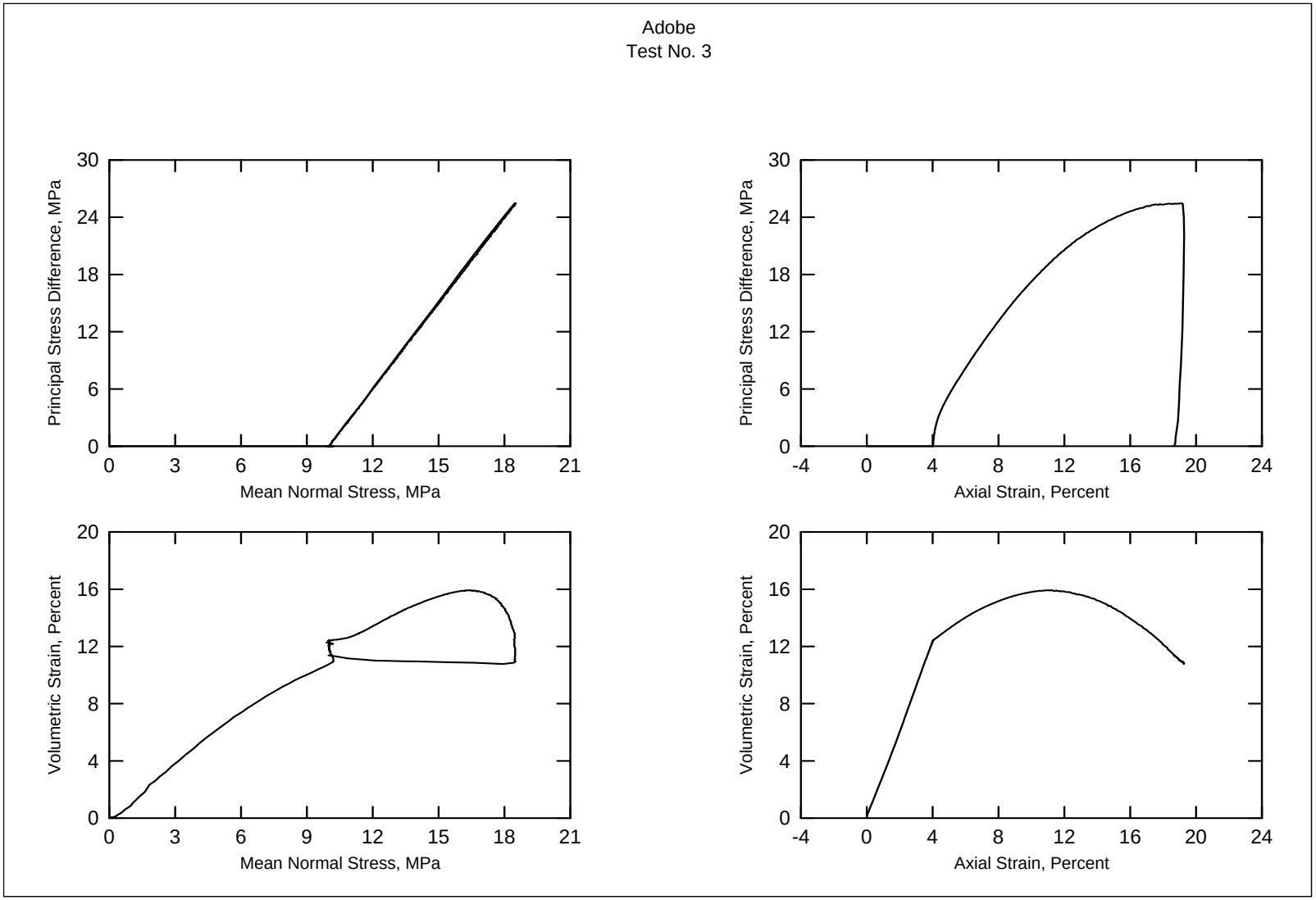
Adobe
Test No. 3
Principal Stress Difference, MPa
Mean Normal Stress, MPa
Principal Stress Difference, MPa
Axial Strain, Percent
Volumetric Strain, Percent
Mean Normal Stress, MPa
Volumetric Strain, Percent
Axial Strain, Percent

Plate 3

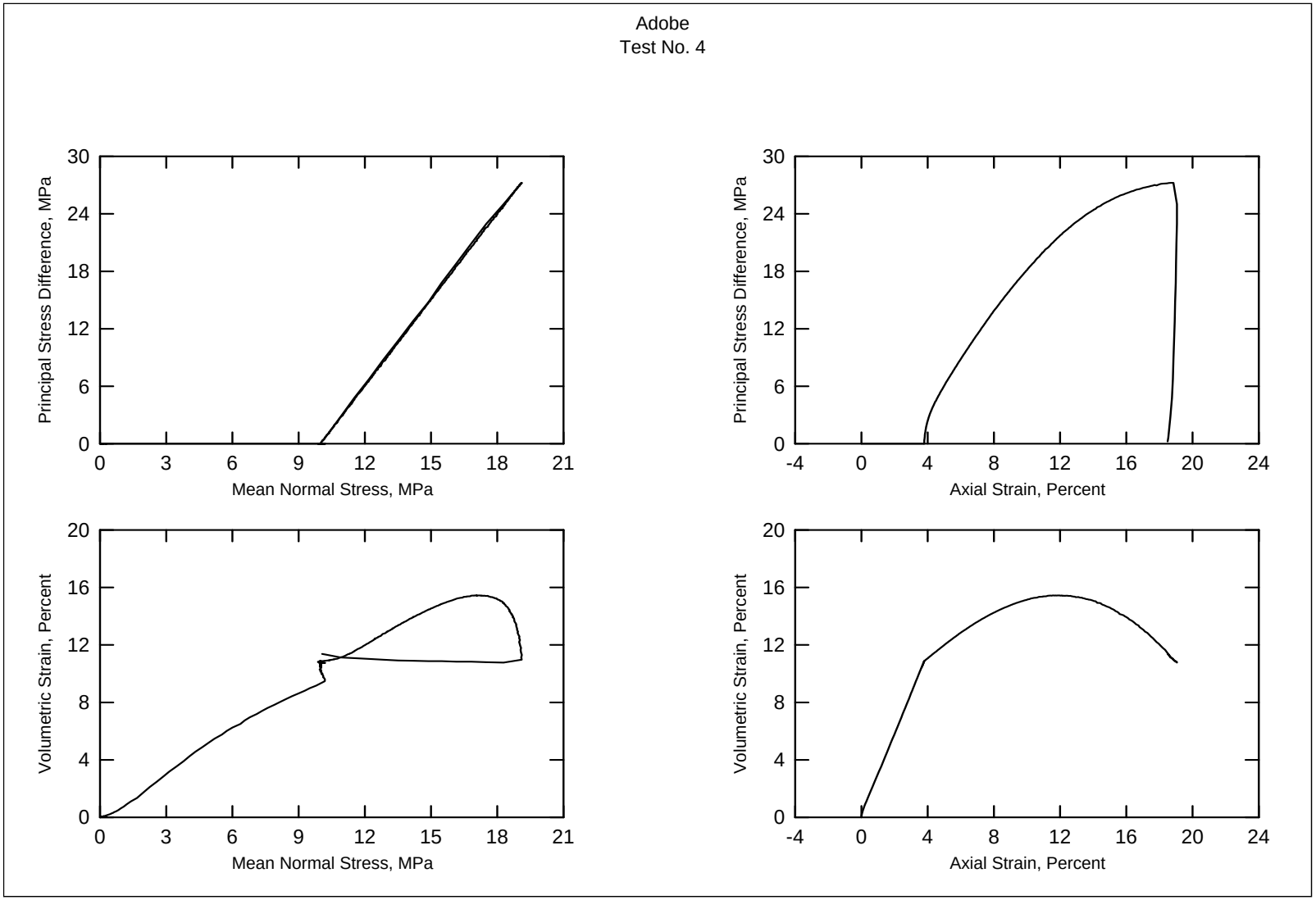
Adobe
Test No. 4
Principal Stress Difference, MPa
Mean Normal Stress, MPa
Principal Stress Difference, MPa
Axial Strain, Percent
Volumetric Strain, Percent
Mean Normal Stress, MPa
Volumetric Strain, Percent
Axial Strain, Percent

Plate 4

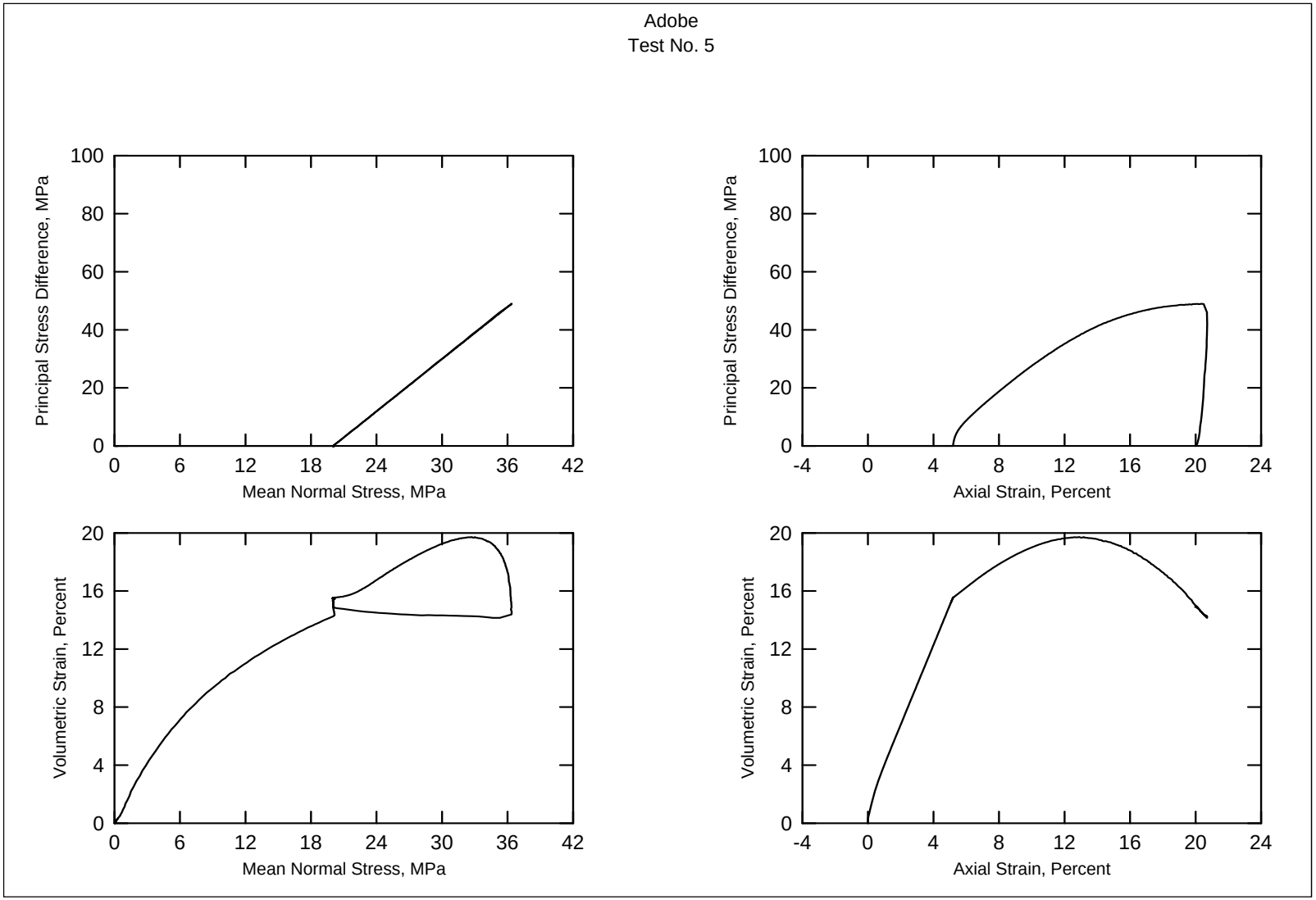
Adobe
Test No. 5
Principal Stress Difference, MPa
Mean Normal Stress, MPa
Principal Stress Difference, MPa
Axial Strain, Percent
Volumetric Strain, Percent
Mean Normal Stress, MPa
Volumetric Strain, Percent
Axial Strain, Percent

Plate 5

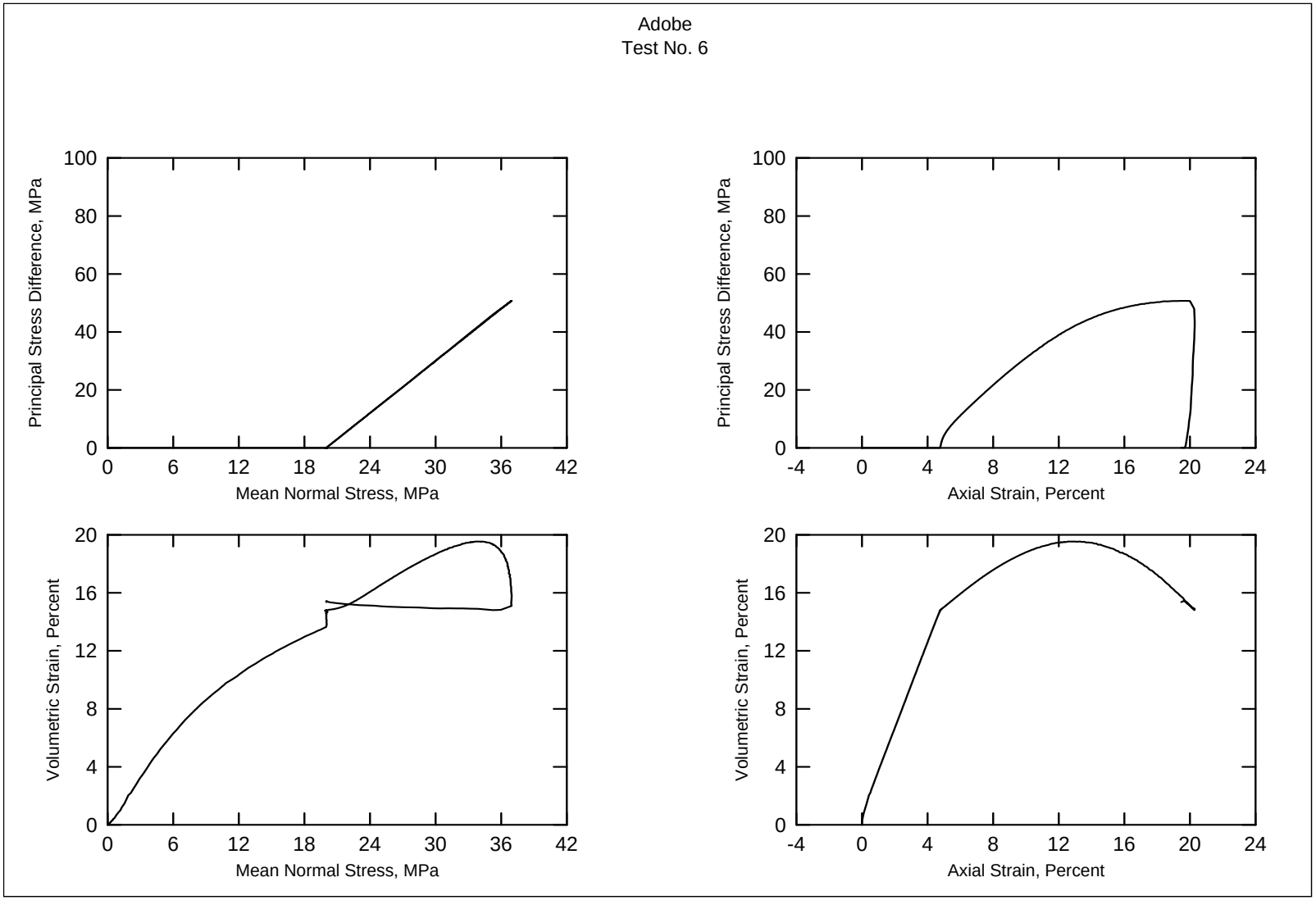
Adobe
Test No. 6
Principal Stress Difference, MPa
Mean Normal Stress, MPa
Principal Stress Difference, MPa
Axial Strain, Percent
Volumetric Strain, Percent
Mean Normal Stress, MPa
Volumetric Strain, Percent
Axial Strain, Percent

Plate 6

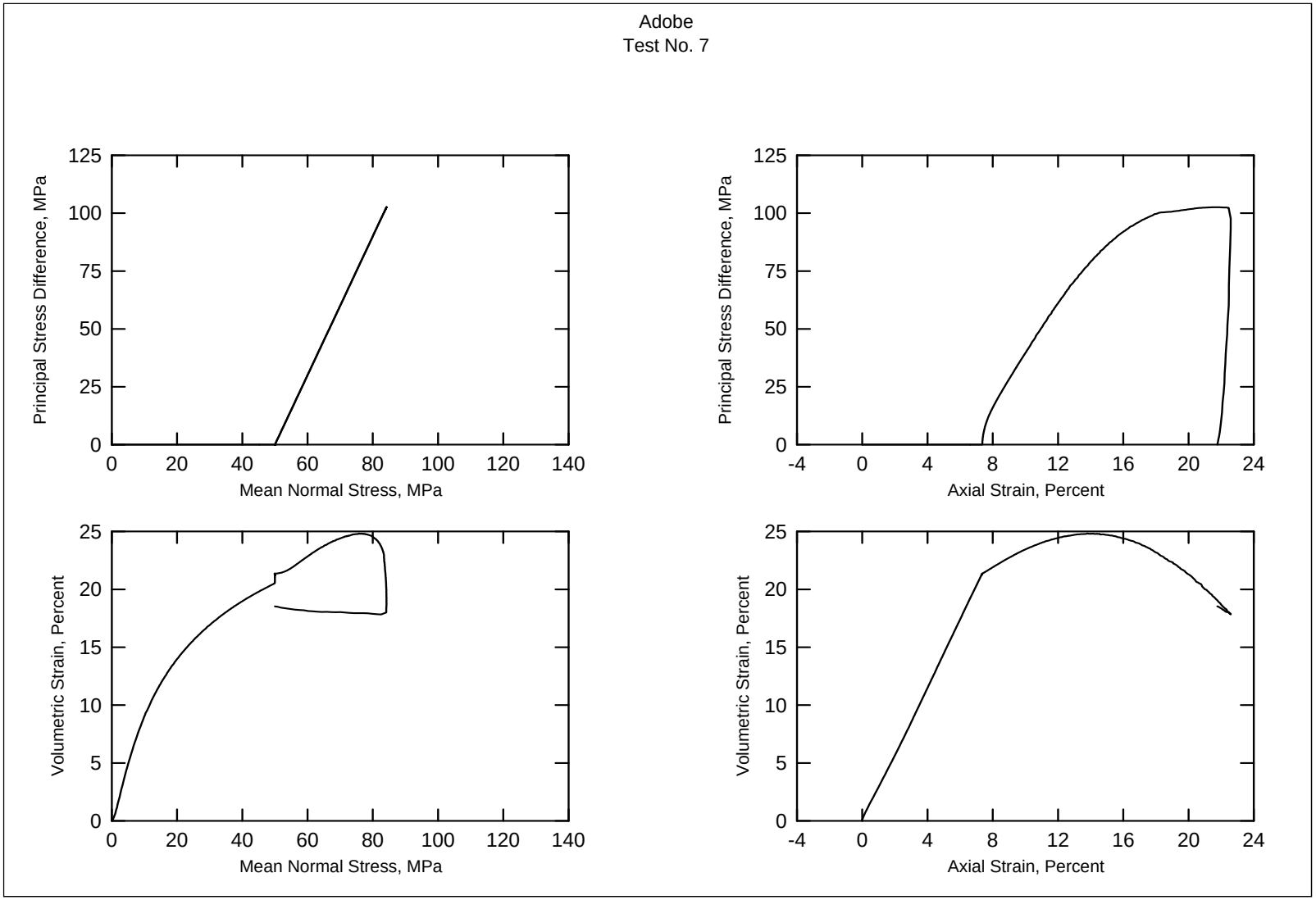
Adobe
Test No. 7
Principal Stress Difference, MPa
Mean Normal Stress, MPa
Principal Stress Difference, MPa
Axial Strain, Percent
Volumetric Strain, Percent
Mean Normal Stress, MPa
Volumetric Strain, Percent
Axial Strain, Percent

Plate 7

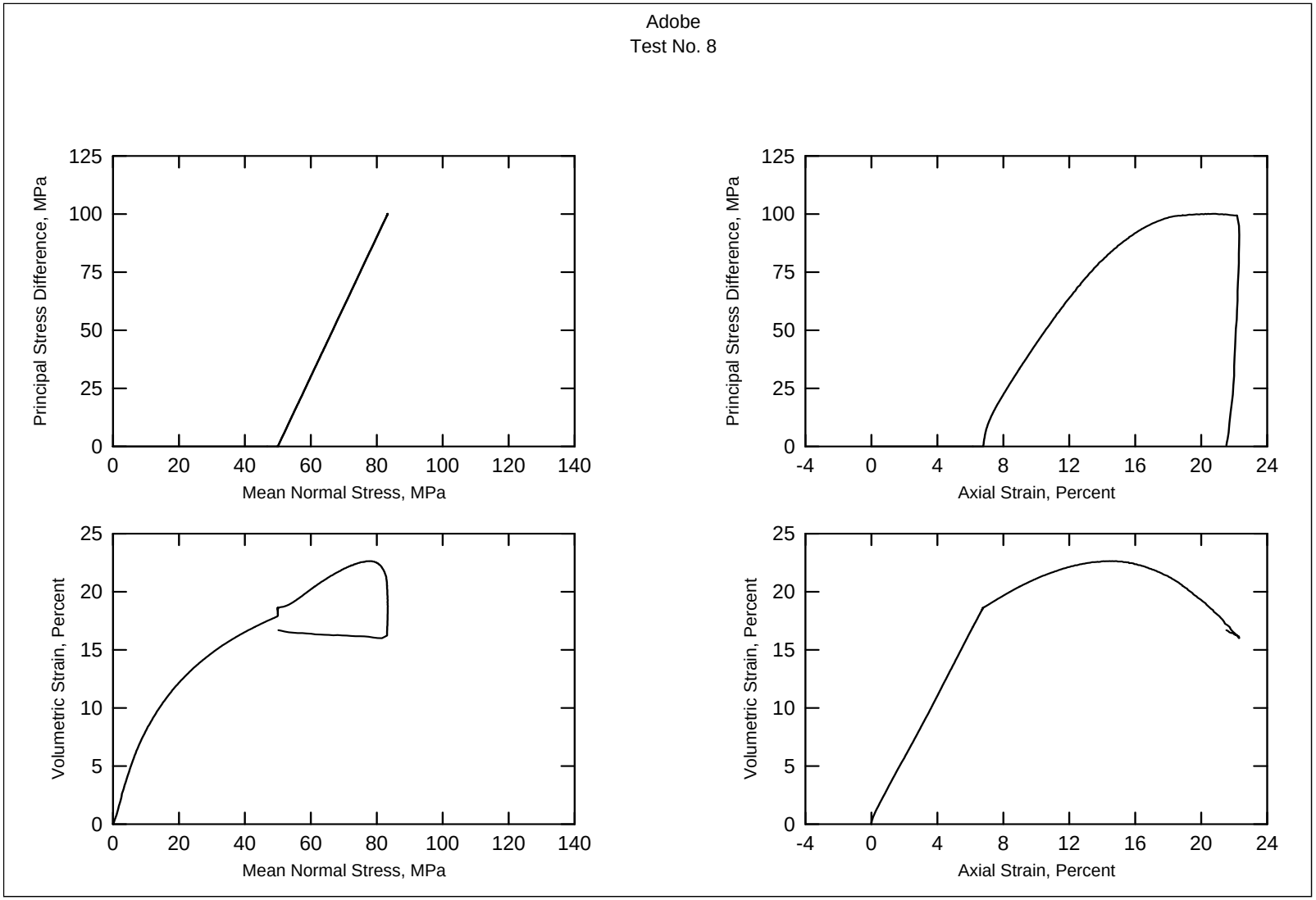
Adobe
Test No. 8
Principal Stress Difference, MPa
Mean Normal Stress, MPa
Principal Stress Difference, MPa
Axial Strain, Percent
Volumetric Strain, Percent
Mean Normal Stress, MPa
Volumetric Strain, Percent
Axial Strain, Percent

Plate 8

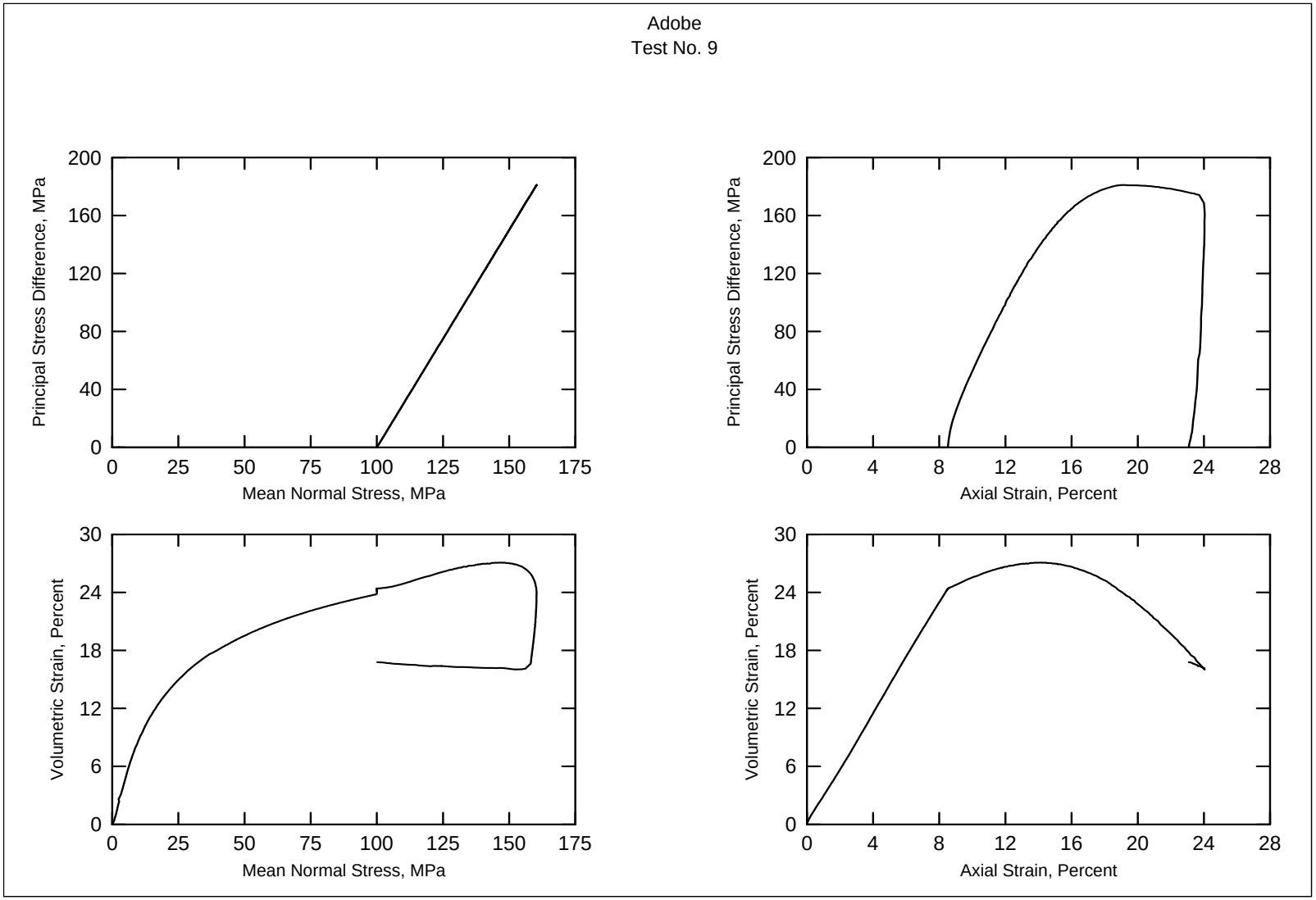
Adobe
Test No. 9
Principal Stress Difference, MPa
Mean Normal Stress, MPa
Principal Stress Difference, MPa
Axial Strain, Percent
Volumetric Strain, Percent
Mean Normal Stress, MPa
Volumetric Strain, Percent
Axial Strain, Percent

Plate 9

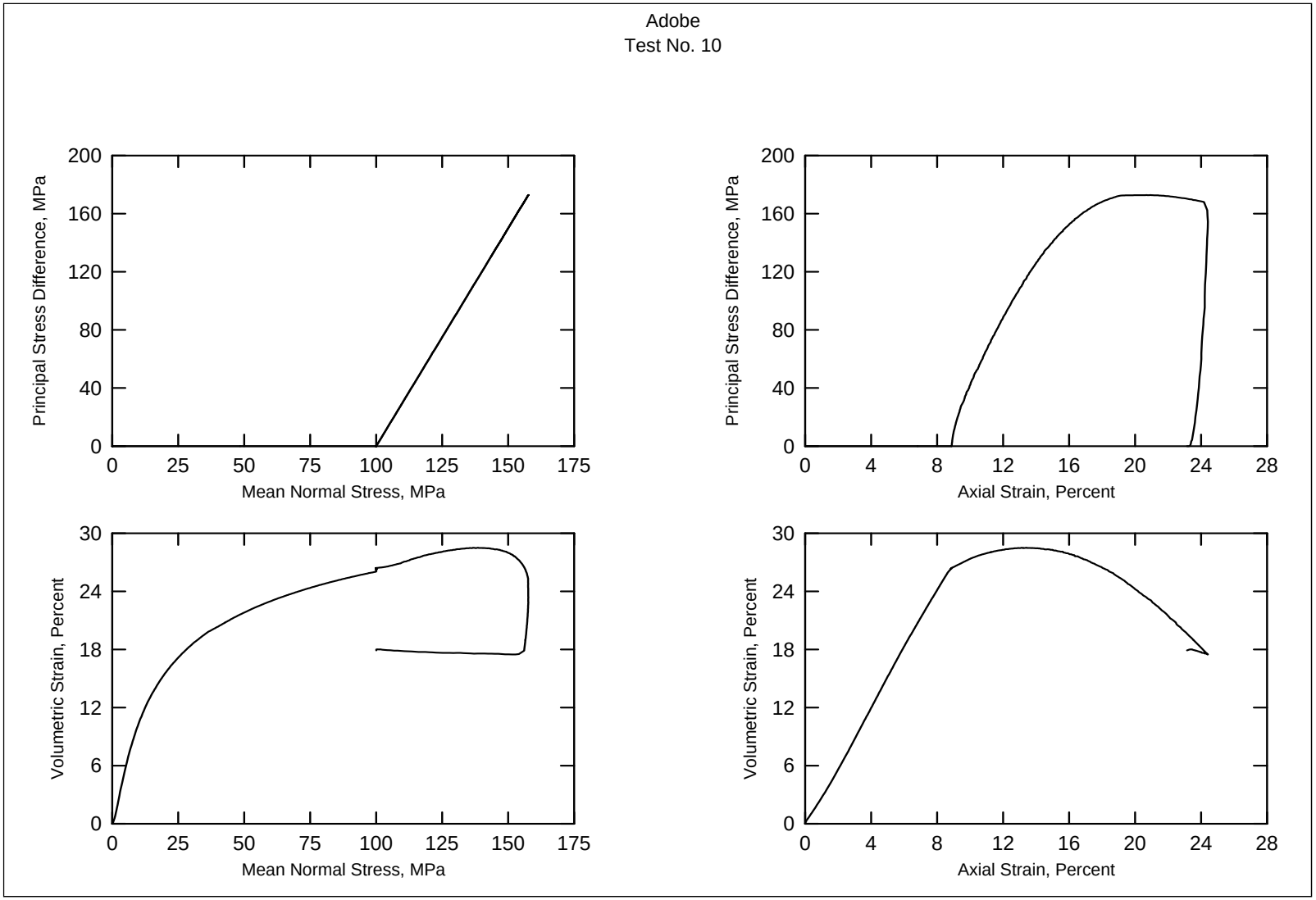
Adobe
Test No. 10
Principal Stress Difference, MPa
Mean Normal Stress, MPa
Principal Stress Difference, MPa
Axial Strain, Percent
Volumetric Strain, Percent
Mean Normal Stress, MPa
Volumetric Strain, Percent
Axial Strain, Percent

Plate 10

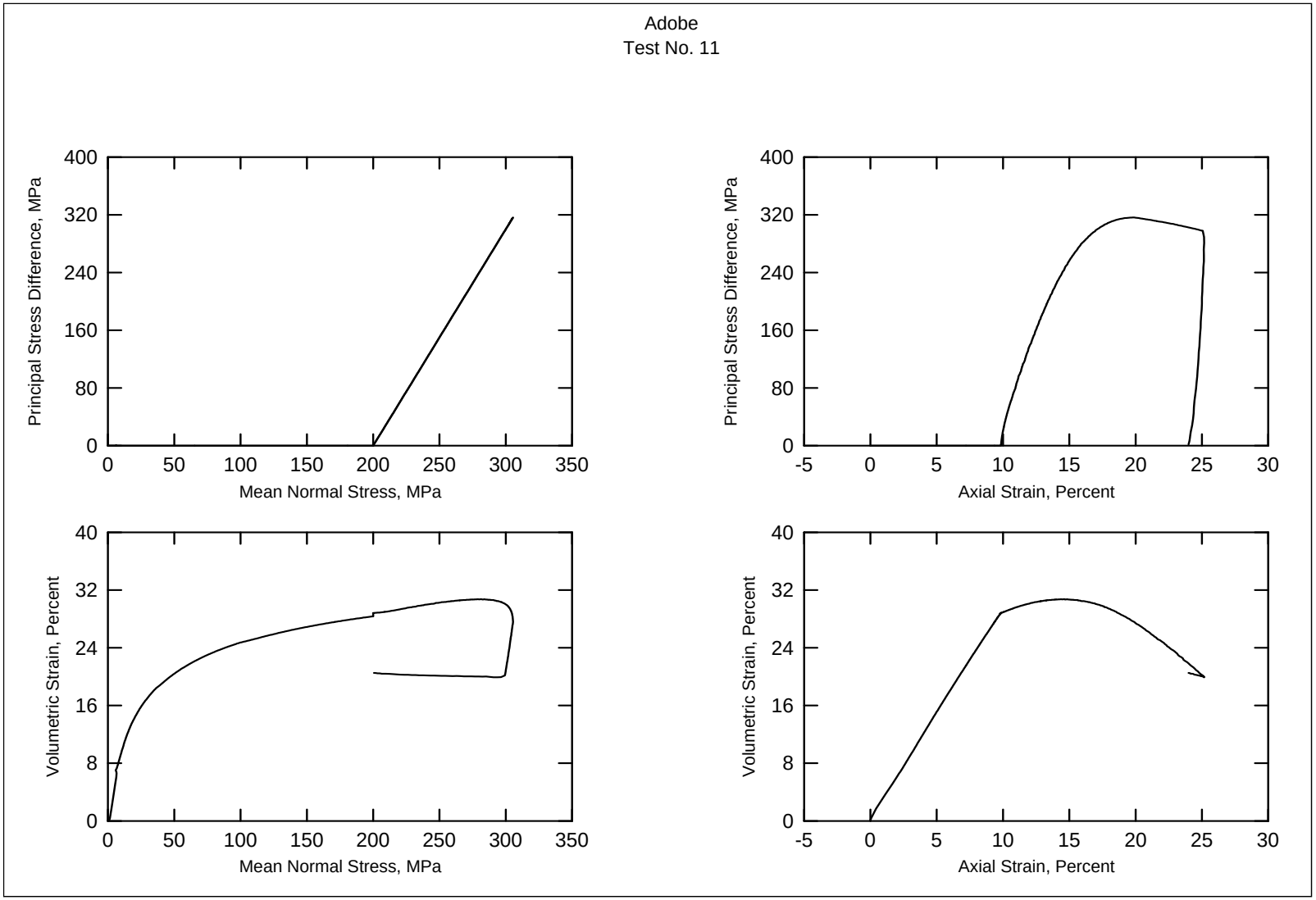
Adobe
Test No. 11
Principal Stress Difference, MPa
Mean Normal Stress, MPa
Principal Stress Difference, MPa
Axial Strain, Percent
Volumetric Strain, Percent
Mean Normal Stress, MPa
Volumetric Strain, Percent
Axial Strain, Percent

Plate 11

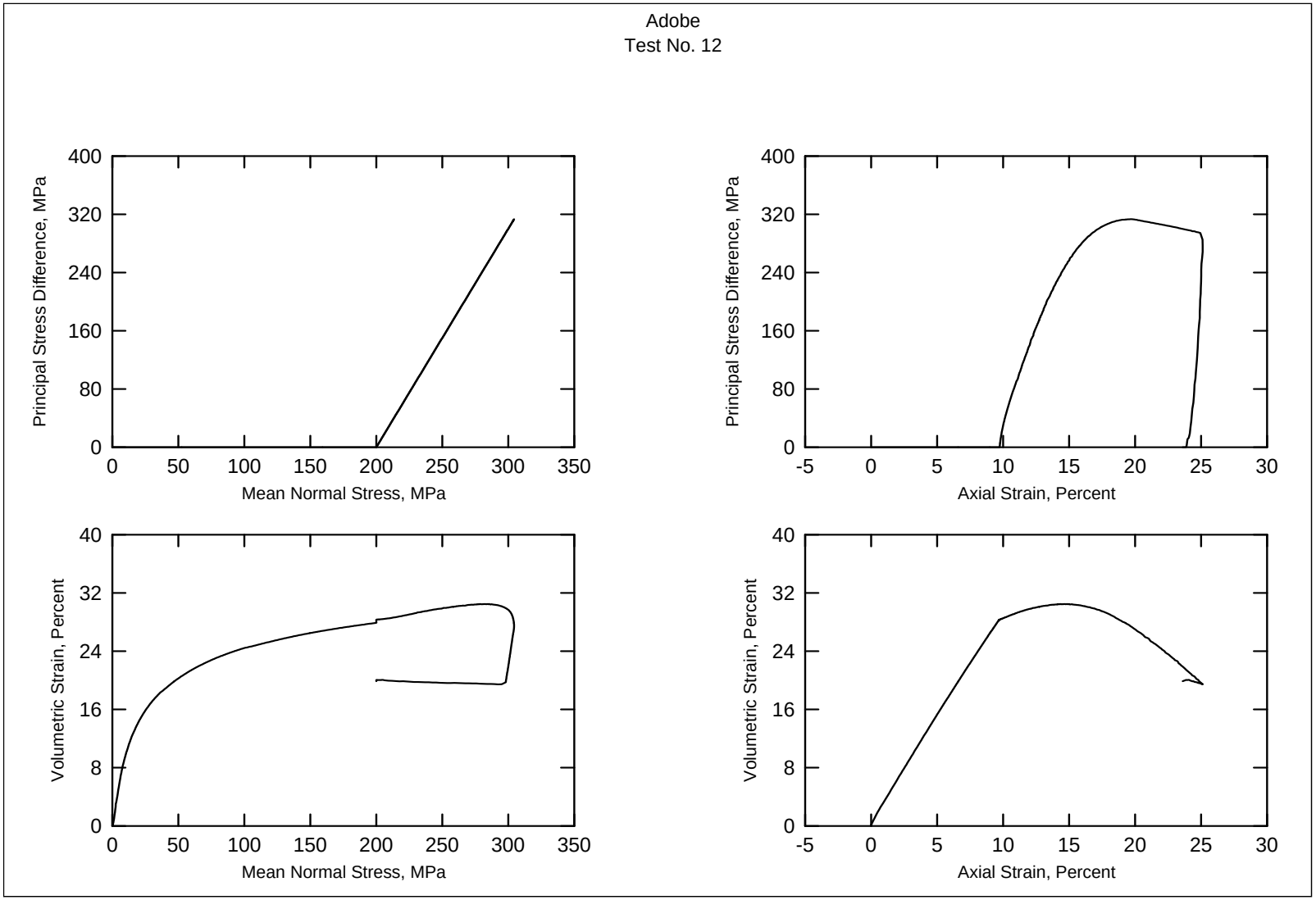
Adobe
Test No. 12
Principal Stress Difference, MPa
Mean Normal Stress, MPa
Principal Stress Difference, MPa
Axial Strain, Percent
Volumetric Strain, Percent
Mean Normal Stress, MPa
Volumetric Strain, Percent
Axial Strain, Percent

Plate 12

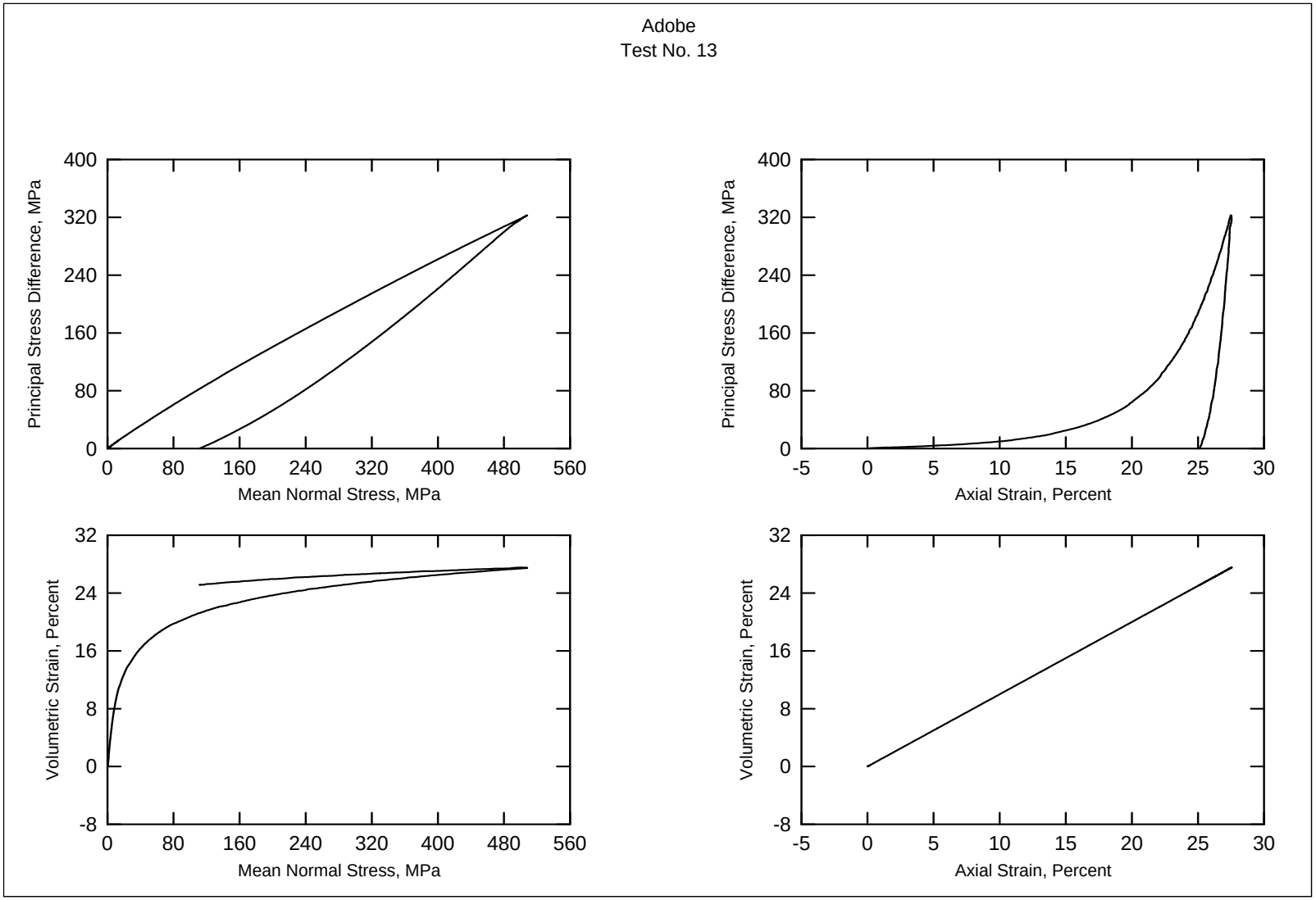
Adobe
Test No. 13
Principal Stress Difference, MPa
Mean Normal Stress, MPa
Principal Stress Difference, MPa
Axial Strain, Percent
Volumetric Strain, Percent
Mean Normal Stress, MPa
Volumetric Strain, Percent
Axial Strain, Percent

Plate 13

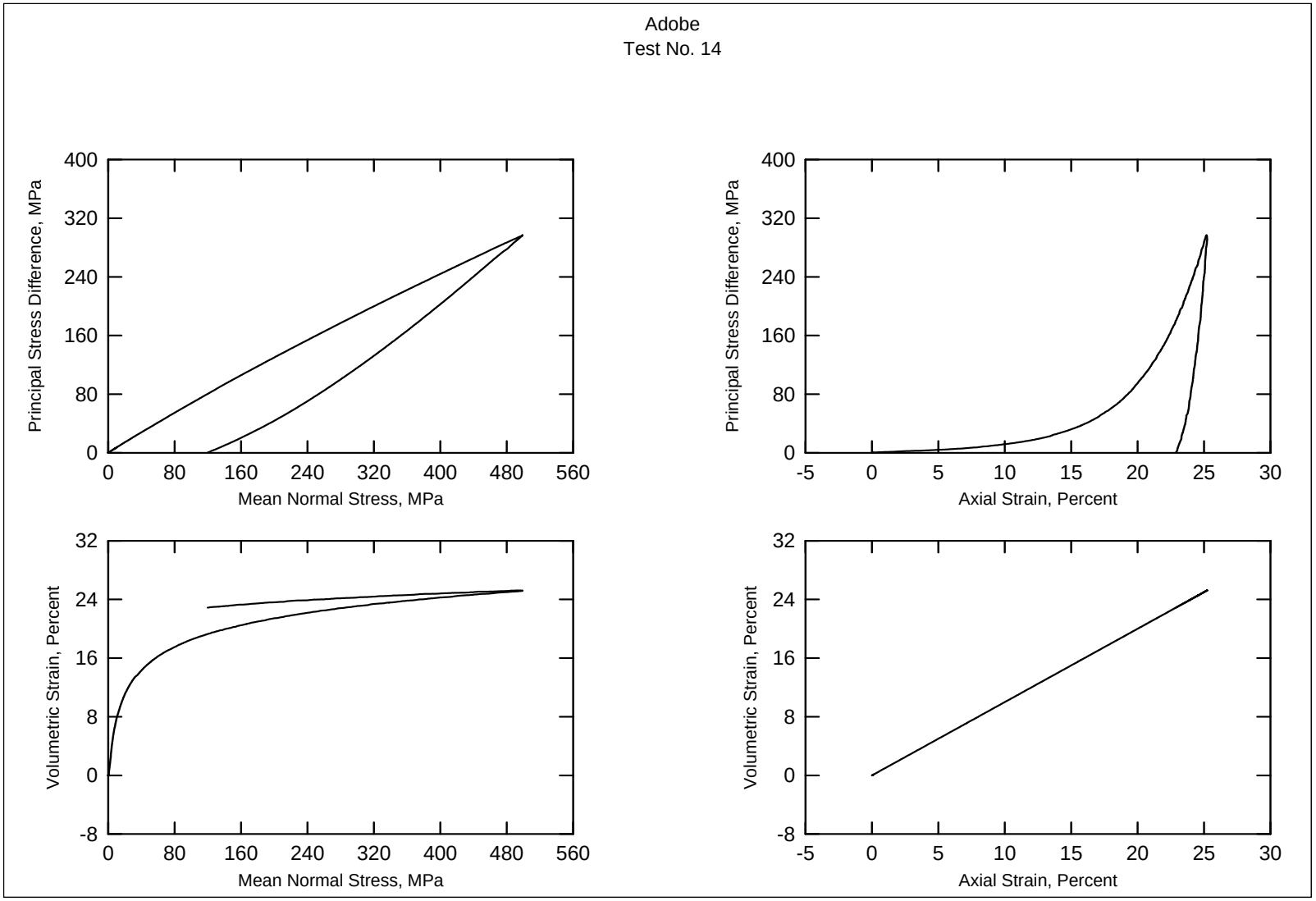
Adobe
Test No. 14
Principal Stress Difference, MPa
Mean Normal Stress, MPa
Principal Stress Difference, MPa
Axial Strain, Percent
Volumetric Strain, Percent
Mean Normal Stress, MPa
Volumetric Strain, Percent
Axial Strain, Percent

Plate 14

REPORT DOCUMENTATION PAGE

Form Approved
OMB No. 0704-0188

1. REPORT DATE *(DD-MM-YYYY)*	2. REPORT TYPE	3. DATES COVERED *(From - To)*
July 2012	Final	

4. TITLE AND SUBTITLE

Laboratory Characterization of Adobe (Scottsdale)

5a. CONTRACT NUMBER

5b. GRANT NUMBER

5c. PROGRAM ELEMENT NUMBER

6. AUTHOR(S)

Hannah B. Beatty, Steven S. Graham, Rayment E. Moxley, Stephen A. Akers, and Paul A. Reed

5d. PROJECT NUMBER

5e. TASK NUMBER

5f. WORK UNIT NUMBER

7. PERFORMING ORGANIZATION NAME(S) AND ADDRESS(ES)

U.S. Army Engineer Research and Development Center
Geotechnical and Structures Laboratory
3909 Halls Ferry Road
Vicksburg, MS 39180-6199

8. PERFORMING ORGANIZATION REPORT NUMBER

ERDC/GSL TR-12-26

9. SPONSORING / MONITORING AGENCY NAME(S) AND ADDRESS(ES)

Headquarters, U.S. Army Corps of Engineers
441 G Street, NW
Washington, DC 20314-1000

10. SPONSOR/MONITOR'S ACRONYM(S)

USACE

11. SPONSOR/MONITOR'S REPORT NUMBER(S)

12. DISTRIBUTION / AVAILABILITY STATEMENT

Approved for public release; distribution is unlimited.

13. SUPPLEMENTARY NOTES

14. ABSTRACT

Personnel of the Geotechnical and Structures Laboratory, U.S. Army Engineer Research and Development Center, Vicksburg, Mississippi, conducted a laboratory investigation to characterize the strength and constitutive property behavior of an adobe from Scottsdale, Arizona. Twenty-one mechanical property tests, consisting of 12 triaxial compression (TXC) tests, two uniaxial strain (UX) tests, and seven unconfined compression (UC) tests, were successfully completed. In addition to the mechanical property tests, nondestructive pulse-velocity measurements were performed on each specimen. The TXC tests exhibited a continuous increase in maximum principal stress difference with increasing confining stress. A compression failure surface was developed from the UC and TXC test results. The UX stress-strain responses exhibited continuous increases in compaction up to the applied peak stresses and did not achieve full saturation.

15. SUBJECT TERMS

Adobe
Compression tests
Material characterization
Mechanical properties

16. SECURITY CLASSIFICATION OF:			17. LIMITATION OF ABSTRACT	18. NUMBER OF PAGES	19a. NAME OF RESPONSIBLE PERSON
a. REPORT	b. ABSTRACT	c. THIS PAGE			19b. TELEPHONE NUMBER *(include area code)*
UNCLASSIFIED	UNCLASSIFIED	UNCLASSIFIED	UNCLASSIFIED	49	